

**Space Telescope Observations of Warm Dust
in Low Surface Brightness Galaxies**

by

Pa Chia Thao

*Submitted to the Department of Astronomy at Mount Holyoke College
with the purpose of honors consideration*

Thesis Advisor: Dr. Jason Young

December 2017

Declaration of Authorship

I hereby certify that this thesis has been composed by me and is based on my own work, unless stated otherwise. No other person's work has been used without due acknowledgement in this thesis. All references and verbatim extracts have been quoted, and all sources of information, including graphs and data sets have been specifically acknowledged.

Signed:

Date:

“Once you make a decision, the universe conspires to make it happen.”

~ Ralph Waldo Emerson

Abstract

Blue in color, a low star formation rate, dark matter dominated, and low in metallicity, low surface brightness (LSB) galaxies questions the current understanding of galactic formation by representing an alternative to the classical Hubble sequence. LSB galaxies are proposed to be the result of galactic overfeeding as high velocity clouds (HVC) weaken the metal content in gas, hindering the process of forming more stars. Although HVCs can dilute the metallicity content, it cannot destroy dust grains. Without HVC dilution, it is expected that there is a correlation between metallicity and dust. To get the dust content, we created warm dust maps using the Independent Component Analysis, first introduced by Meidt et al. (2012), on the Spitzer IRAC 3.6 and 4.5 μm images on 10 LSB galaxies: UGC 628, UGC 731, UGC 11748, UGC 11820, UGC 1230, F415-3, F583-5, F584-2, UGC 5709, F563-V2. The images were decomposed to trace either the old stellar population or the contaminant sources of emission, which included Polycyclic Aromatic Hydrocarbons, warm dust, intermediate-age asymptotic giant branch stars and red supergiant stars. We find that in our sample, warm dust is present in all the galaxies, old stellar populations reside in the center and unlike their high surface brightness (HSB) galaxy counterparts, there are a small number of larger HII regions that do not show preference to the center. In the future, we hope to refine our methods, increase our sample size, and convert our contaminant images into dust maps to compare with the metallicity content of each galaxy. Such studies will determine if low surface brightness galaxies are the outcome of galactic overfeeding and provide insight into the evolutionary path of these galaxies.

Acknowledgements

I offer my utmost gratitude to my advisor, Dr. Jason Young. Without his guidance, expertise, and persistence, this thesis would of never been possible. Thank you for giving me the opportunity to embark on this journey and being patient as I learned how to code in a new language. You have made such a difference in my life and I feel tremendously fortunate to have you as my advisor.

I am grateful for the Lynk Universal Application Funding and their generous support.

A very special thanks to my committee members, Dr. Darby Dyar and Dr. Spencer Smith for taking their time to read this thesis and for all their valuable comments.

Many thanks to Miguel Querejeta, for pointing me towards the right direction in completing this thesis and promptly answering all my many questions.

I would also like to acknowledge all my professors here at Mount Holyoke College, as well as professors in the greater Five Colleges, for fostering my love for astronomy and challenging me to keep questioning the world around me.

I am grateful to have had so many amazing mentors throughout this journey. A special thank you to Dr. Andrew Mann, who pushed me to grow so much as a researcher.

I would also like to thank my parents and my four brothers for their continuous support and unconditional love throughout my life. Finally, to my best friend, Chase, whose constant encouragement and confidence gave me the motivation to finish this.

Contents

Declaration of Authorship	ii
Abstract	iv
Acknowledgements	v
List of Figures	ix
List of Tables	x
Abbreviations	xi
Chapter 1: Introduction	1
1.1 Freeman’s Law	2
1.2 Proposed Causes of Low Surface Brightness Galaxies	4
1.2.1 Isolation	5
1.2.2 Dark Matter	6
1.2.3 Galactic Overfeeding	8
1.3 The Proposed Study	9
Chapter 2: Background	13
2.1 The First LSB Galaxy: Malin 1	13
2.2 Measurements of Brightness	15
2.3 Features of LSB Galaxies in Sample	17
2.3.1 Spiral Galaxies	17
2.3.2 Blue Colored	18
2.3.3 Dark Matter -Dominated	19

2.3.4	Low Star Formation Rate	20
2.3.5	Low Metallicity	20
2.4	Significance of Low Surface Brightness Galaxies	21
2.4.1	Quiescent Evolution	21
2.4.2	Dark Matter	21
2.4.3	Missing Mass Problem	22
2.4.4	Star Formation Activity in Low Metallicity Environments	22
Chapter 3: Materials and Methodology.....		24
3.1	Infrared	24
3.2	Spitzer Space Telescope	27
3.3	Contaminants	27
3.3.1	Polycyclic Aromatic Hydrocarbon.....	27
3.3.2	Warm Dust	28
3.3.3	AGB and RSG Stars.....	29
3.4	Independent Component Analysis.....	30
3.5	Procedure	34
3.6	Replication and Comparison	37
3.7	Target Selection.....	38
Chapter 4: Results.....		41
4.1	Analysis	41
4.1.1	UGC 628.....	44
4.1.2	UGC 731.....	45
4.1.3	UGC 11748.....	45
4.1.4	UGC 11820.....	46
4.1.5	UGC 1230.....	46
4.1.6	F415-3	47
4.1.7	F583-5	47
4.1.8	F584-2	48
4.1.9	UGC 5709.....	48
4.1.10	F563-V2	48

Chapter 5: Conclusion and Discussion	50
5.1 Dust Emission Content	50
5.2 Location of Old Stellar Population	51
5.3 Location of Star Formation.....	52
5.4 Improvements	52
5.4.1 Signal-to-Noise Threshold	52
5.4.2 Masking Foreground Stars	53
5.4.3 Applying a Second Iteration of ICA.....	53
5.5 Future Work.....	54
5.5.1 Dust Content Maps.....	54
5.5.2 Mass Maps	54
5.5.3 Mass-to-Light Ratio	54
5.6 Summary.....	55
 Bibliography	 57
 Appendix.....	 65
Appendix A Python code to convolve images.....	65
Appendix B Python code to perform background subtraction	67
Appendix C C++ code to perform ICA	69

List of Figures

FIGURE 1.1 Hubble Tuning Fork	1
FIGURE 1.2 Space density as a function of central surface brightness (Bothun et al. 1997)	3
FIGURE 1.3 Central surface brightness as a function of b-v (Bothun et al. 1997)..	4
FIGURE 1.4 The enclosed mass-to-light ratio as a function of central surface brightness (McGaugh)	6
FIGURE 1.5 Rotation curves of UGC 128 and NGC 2403 (de Blok & McGaugh 1996)	7
FIGURE 1.6 High velocity clouds in the Milky Way (Wakker 1999)	8
FIGURE 1.7 Different hypothesis for LSB galaxies	9
FIGURE 1.8 Correlation between H-alpha extinction with star formation rate, metallicity, and stellar mass (Garn & Best 2010)	10
FIGURE 1.9 Diagram of the overarching goal of this project.....	11
FIGURE 2.1 Malin 1.....	14
FIGURE 2.2 Anatomy of the Milky Way.....	17
FIGURE 2.3 Fractional distributions of 21-cm velocity widths for sample of LSB and HSB galaxies (Bothun et al. 1997).....	18
FIGURE 3.1 Black body curve.....	24
FIGURE 3.2 Spitzer Space Telescope	26
FIGURE 3.3 Polycyclic Aromatic Hydrocarbon	27
FIGURE 3.4 Evolutionary tracks off the Main Sequence	29
FIGURE 4.1 Different HII regions in UGC 628 labeled (Young et al. 2015).....	44
FIGURE 4.2 UGC 1230 taken in different wavelengths	46

List of Tables

TABLE 3.1 Different sources in IRAC images and corresponding color ranges (Querejeta et al. 2015)	33
TABLE 3.2 Comparison of stellar and non-stellar images of NGC 2976	38
TABLE 3.3 List of sample galaxies.....	40
TABLE 4.1 Comparison of the 3.6 μ m, stellar, and non-stellar images.....	41
TABLE 4.2 Summary of explanation for different combinations of outcome	41

Abbreviations

LSB	Low Surface Brightness
HSB	High Surface Brightness
ICA	Independent Component Analysis
PCA	Principal Component Analysis
SFR	Star Formation Rate
RPS	Ram Pressure Stripping
ICM	Intracluster Medium
S⁴G	Spitzer Survey of Stellar Structures in Galaxies
MUSCEL	MUltiwavelength observations of the Structure, Chemistry and Evolution of LSB galaxies
PAH	Polycyclic Aromatic Hydrocarbons
HVC	High Velocity Clouds
SST	Spitzer Space Telescope
IRAC	Infrared Array Camera
IRS	Infrared Spectrograph
MIPS	Multiband Imaging Photometer for Spitzer
IRSA	Infrared Science Archive
AGB	Asymptotic Giant Branch
RSG	Red Supergiants
BSS	Blind Source Separation
CLT	Central Limit Theorem
PBCD	Post Basic Calibrated Data
PSF	Point Spread Function
VIRUS-P	Visible Integral-field Replicable Unit Spectrograph - Prototype

TO MY MOM,

whose perseverance and hard work

will always inspire me to do better

and

TO CHASE,

thank you for being such a light in my life.

Chapter 1: Introduction

If you get the chance to look up into the sky on a cloudless night, in an area with little light pollution, you will see one of nature’s most breathtaking natural phenomena: a band of stars spread across the sky. This band is our galaxy, the Milky Way, which is just one out of the billions of galaxies in the universe. A galaxy is a system of stars, gas, dust, and dark matter, all gravitationally bound to each other and orbiting a common center. Galaxies vary in shape and size with distinct features; not one is exactly alike.

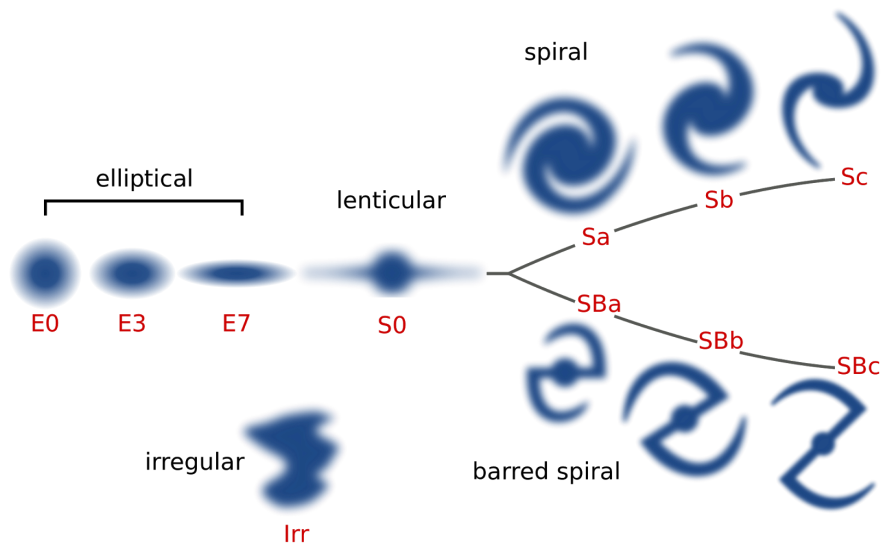


FIGURE 1.1: Hubble Tuning Fork.

To classify how galaxies evolve over time, astronomer Edwin Hubble – a pioneer in observational cosmology – observed the morphology of galaxies and created the **Hubble Sequence** that is known more colloquially as, the “Hubble tuning fork diagram.” As seen in **Figure 1.1**, the scheme divides galaxies into three classes based on their visual appearance: elliptical, lenticular, and spiral. Galaxies that do not fit the characteristics of these three respective classes are grouped as irregulars. Different types of galaxies vary in terms of their

relative stellar and gas contents, star formation histories, and their internal motions. Even though this simple classification is still commonly used today, it fails to include a true census of all types of galaxies, along with this thesis's focus, low surface brightness (LSB) galaxies, diffuse galaxies that have surface brightness values greater than $22 \text{ mag arcsec}^{-2}$.

1.1 Freeman's Law

Like Hubble, in an attempt to categorize galaxies, in 1970, astronomer Ken Freeman analyzed the photometry of several spiral galaxies' disks. Out of the 36 galaxies in his sample, 28 fell within the same central surface brightness range, $\mu_0 = 21.65 \pm 0.35 \text{ mag arcsec}^{-2}$. This result became known as **Freeman's Law** and has become prominent in astronomy, having been cited over 700 times!

Yet, there were many who remained skeptical of Freeman's outcome. Bothun et al. (1997) argued that this law implies that all disk galaxies must then undergo the same physical processes of disk galaxy formation and evolution in order to have the same central surface brightness, which is a very specific and arbitrary value. However, it is known that there is variation in star formation history. Even though all stars form from rotating giant clouds of gas and dust, they vary in temperature, brightness, color, metallicity, structure, size, and age. With different life cycles, it can be inferred that galaxies must also vary in surface brightness.

As the central surface brightness of galaxies, μ_0 , approaches the sky brightness level, the number of galaxies rapidly declines. Swiss astronomer Fritz Zwicky, who made numerous contributions to theoretical and observational astronomy, noticed this trend and first proposed that the night sky must then restrict our view of the kind of galaxies that could be discovered

(Bothun et al. 1997). Disney (1976) investigated the depth of this selection's effect and McGaugh et al. (1995) confirmed that these effects were real. A reproduction of McGaugh's findings (**Figure 1.2**) shows the surface brightness distribution suggested by Freeman's Law using a solid curve. If this trend is true, then all galaxies would follow the line. However, there are many points to the left of the line, contradicting Freeman's Law. These numerous hidden objects are called low surface brightness (LSB) galaxies.

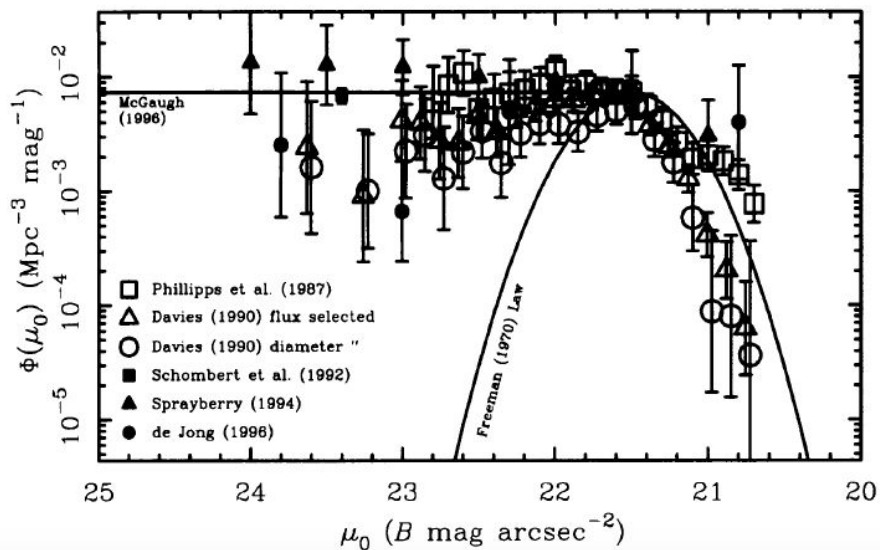


FIGURE 1.2: The space density of galaxies as a function of central surface brightness. The solid curve line is the surface brightness distribution that supports Freeman's Law. The many points to the left of this line are LSB galaxies (Bothun et al. 1997).

Because galaxy detection is based on the galaxies that can be seen, a proper census of all types of galaxies has been lacking for years. Hubble predicted this shortcoming:

Subdivision of non-galactic nebulae is a much more difficult problem. At present and for many years to come, their classification must rest solely upon the simple inspection of photographic images, and will be confused, by the use of the telescopes of widely differing scales and resolving powers. Whatever selection of types is made, longer exposures and higher resolving powers will surely cause a reclassification of many individual nebulae.

A true sample of all galaxies in the universe was historically impractical because the ambient night sky, like a filter, blocks out all galaxies with a surface brightness an order of magnitude below it. These unnoticed galaxies were discovered by accident in 1986. LSB galaxies are blue in color, have a low star-formation rate, are dark-matter dominated, and have a low metallicity. This combination represents an alternative path of galaxy evolution that does not lead to the classical Hubble sequence. Astronomers have proposed many hypotheses as to what led LSB galaxies to their current state, which will be explored in the next section.

1.2 Proposed Causes of Low Surface Brightness Galaxies

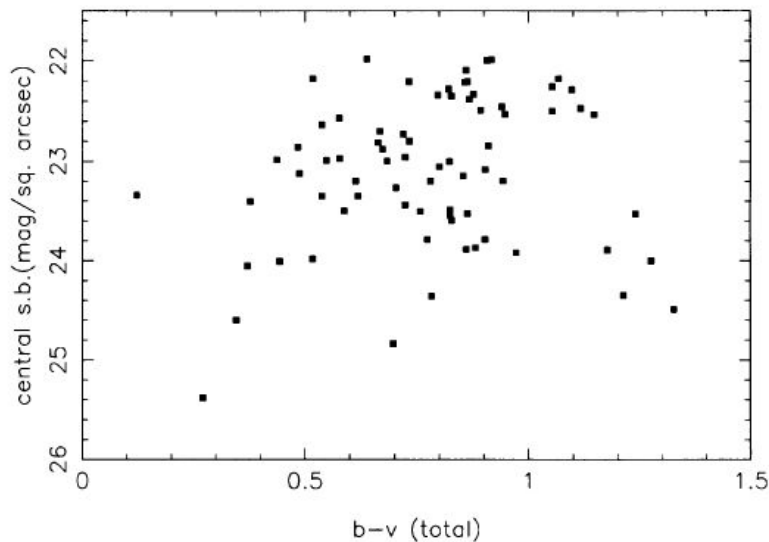


FIGURE 1.3: Central surface brightness as a function of b-v for a sample of LSB galaxies. If LSB galaxies were old remnants, they would have a red color, but not every LSBs are red (Bothun et al. 1997).

LSB galaxies were once believed to result from a “faded disc scenario” – galaxies that were forming stars, but somewhere along the process, faced gas depletion. If this was the case, they would have been unable to form more stars and the color of the galaxies would redden as they age. Although this explains the evolutionary path of red LSB galaxies, to be discussed in

Chapter 2, not all LSB galaxies are red. Most LSB galaxies possess large amounts of hydrogen and are blue in color. A blue-colored galaxy implies that it is still continually forming stars (newly formed stars are blue) and that there are only a few older stars that affect the color (older stars are red). Therefore, not all LSB galaxies can be faded remnants. As supported in **Figure 1.3**, there is not a correlation between central surface brightness and integrated disk color ($b-v$) of LSB galaxies (Bothun et al. 1997). This same conclusion has been supported by several researchers (McGaugh 1992; van der Hulst et al. 1993; McGaugh & Bothun 1994; de Blok et al. 1996).

1.2.1 Isolation

Several authors (e.g., Bothun et al. 1993; Mo et al. 1994) have proposed that isolation could cause the low star formation rate (SFR) in LSB galaxies. Compared to high surface brightness (HSB) galaxies, LSB galaxies tend to be found in more isolated systems and lack companions on scales of < 2 Mpc (Galaz et al. 2011). Forming in isolation affects an LSB galaxy's evolution because interactions and tidal encounters with nearby galaxies are effective in driving star formation. In an analysis of LSB galaxies found in the Sloan Digital Sky Survey (SDSS), Rosenbaum & Bomans (2004) concluded that LSB galaxies located on the edge of the large scale structures are likely to be formed in cosmic voids. de Blok and McGaugh (1996) argued that while this may be true, a LSB galaxy located near a high density region of galaxy distribution can then either ignite star formation (increasing its surface brightness), or remove the LSB galaxy of its low density gas disk (causing the galaxy to become cooler and red in color). In both these scenarios, the resulting galaxy will no longer be identified as an LSB galaxy – potentially explaining why LSB galaxies are found in more isolated systems.

On the other hand, if isolation causes deficiency in star formation, why is it that some LSB galaxies are *not* formed in isolation? Conversely, why are there high surface brightness (HSB) galaxies that do thrive in isolation? Even though isolation is a trend with LSB galaxies, it is hard to argue that the cause of a low star formation rate is simply due to isolation alone.

1.2.2 Dark Matter

While dark matter is present in all galaxies, the content in LSB galaxies is greater when compared to HSB galaxies. In **Figure 1.4**, McGaugh (research website) plots the enclosed mass-to-light ratio as a function of central surface brightness for a sample of galaxies. From this plot, we see that as the the central surface brightness of the galaxy increases (the dimmer it is), the mass-to-light ratio (M/L) increases. A high M/L implies one of two things: either there is a high content of gas or there is a high content of dark matter.

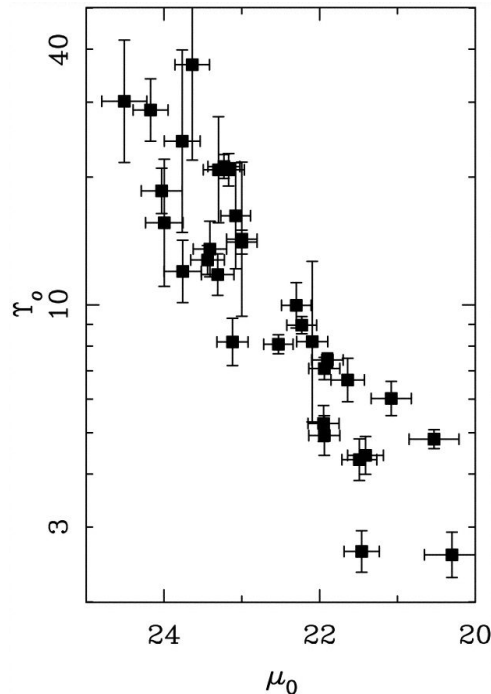


FIGURE 1.4: The enclosed mass-to-light ratio as a function of central surface brightness (McGaugh research website).

The existence of dark matter was first measured by Vera Rubin and Ken Freeman in the 1960-1970s, while working on rotation curves on the Andromeda Galaxy (M31). A rotation curve plots the orbital speeds of the total mass as a function of the radial distance from a galaxy's center. Objects near the center move at a much faster rate in comparison with objects near the edge, so it is expected that as the radius increases, the velocity of the mass will decrease. To their surprise, the mass did not slow down as the radius increased – it kept moving at the same speed. The only explanation for this result was that there was some unforeseen mass in the galaxy, which became known as “dark matter” because it is invisible in the electromagnetic spectrum and does not interact with baryonic matter (ordinary matter). Dark matter halo extend beyond the visible galaxy.

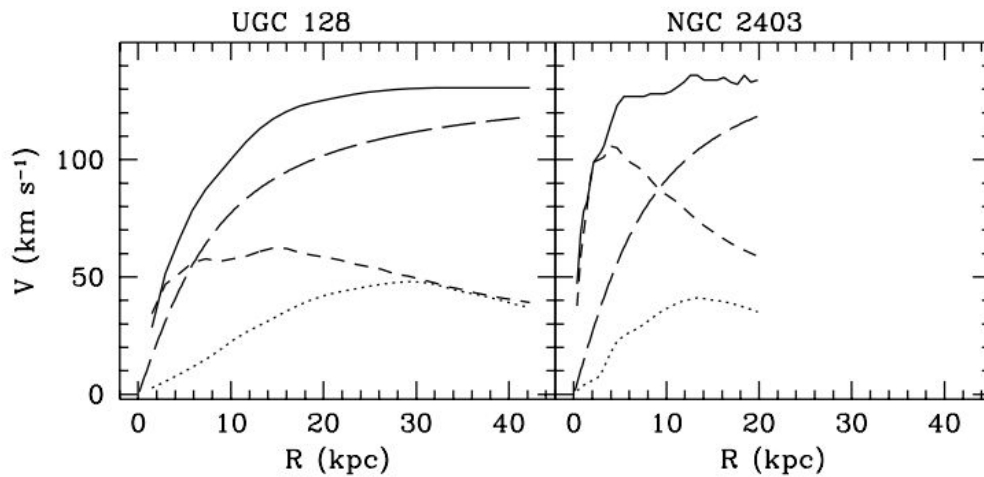


FIGURE 1.5: Comparison of the rotation curves of UGC 128 and NGC 2403. The solid line is the observed rotation curve. The following curves are estimated under the assumption that there is a maximum amount of stars in the disk. The long-dashed line measures the rotation curve of gas. The medium-dashed line is the rotation curve of stars. The small-dashed line is the rotation curve of dark matter (de Blok & McGaugh 1996).

In **Figure 1.5**, de Blok and McGaugh (1996) compared the rotation curves of individual mass components (gas, stars, dark matter) in two galaxies: UGC 128, a LSB galaxy, and NGC 2403, a HSB galaxy. Both are similar in magnitude ($M_B \approx -19$) and maximum velocity ($V_{max} \approx$

134 km s⁻¹). The observed rotation curves, which is represented in the solid curve line in the figure, shows that UGC 128 rises at a much slower rate compared to NGC 2403. The small-dashed line of the two galaxies supports that LSB galaxies inhabit less dense and more extended halos than HSB galaxies. The resulting differences in dark matter halos might then cause the galaxies to lag in star formation and become LSB galaxies. It is difficult to test this hypothesis because dark matter and its interaction with other matter and itself is still not fully understood.

It may also be easier to measure dark matter in LSB galaxies because dark matter dominates near their cores. Conversely, it could be more difficult to measure a reliable halo in HSB galaxies because they do not have strong presences near their cores. Researching LSB galaxies is a window into understanding more about dark matter – a topic that still puzzles the astronomical community.

1.2.3 Galactic Overfeeding

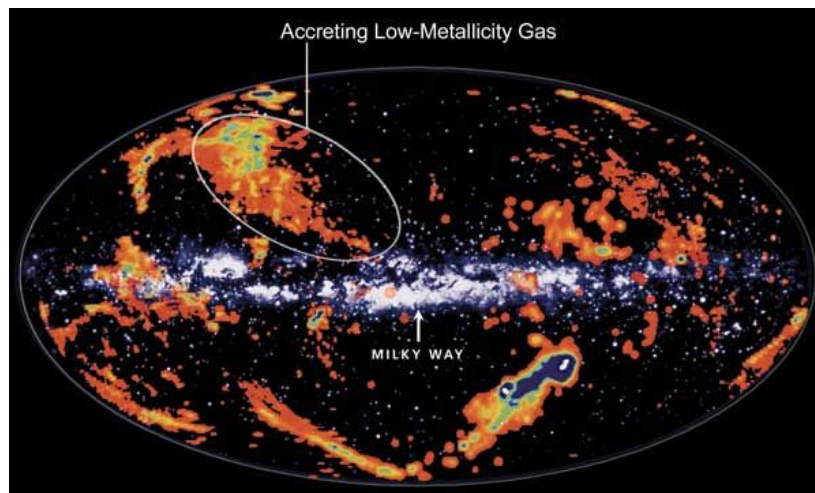


FIGURE 1.6: High velocity clouds found in the Milky Way (Wakker 1999).

Another proposed hypothesis is that LSB galaxies could be receiving more gas than it can consume. Throughout the universe, there are large collections of inflowing gas that are called

high velocity clouds (HVC) (Figure 1.6). Their origin is unknown, though they are believed to be gas remnants pushed away from supernova explosions (dead stars) and falling back down onto the galaxy or gas that has come from another galaxy, as revealed by their chemical composition. Once HVCs are inside a galaxy, their added material can assist in igniting star formation or dilute the metal that is already present in rich gas. Because enriched-metal gas propels star-formation, if HVCs are weakening the metal content in the gas, when a galaxy tries to form more stars, the process of creating new stars will be hindered – resulting in galactic overfeeding (Young et al. 2015).

The different hypotheses for the causes of LSB galaxies are summarized below:

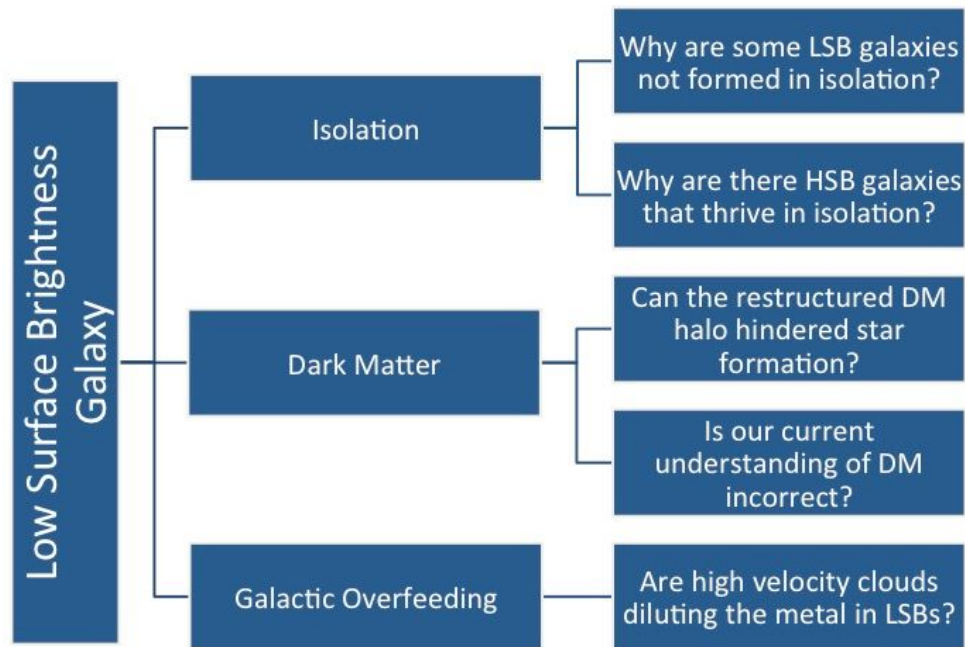


FIGURE 1.7: Different hypothesis for LSB galaxies and corresponding questions (this thesis).

1.3 The Proposed Study

The study of dust and metal contents of LSB galaxies can reveal significant clues to their star formation history. Although high velocity clouds (HVC) dilutes the metallicity content, they

cannot destroy the dust grains. Dust is formed in stars and is returned back to the interstellar medium through supernovae or stellar winds. As seen in **Figure 1.8**, there is a positive correlation between dust extinction with star formation rate, metallicity, and stellar mass. A galaxy that has not been forming many stars would be expected to have low metallicity and poor dust content (Garn & Best 2010). Therefore, dust and metallicity provides a cumulative record of past star formation and chemical history. A LSB galaxy that has a lot of dust and high metallicity is likely not overfed, while a LSB galaxy with a lot of dust and low metallicity was overfed.

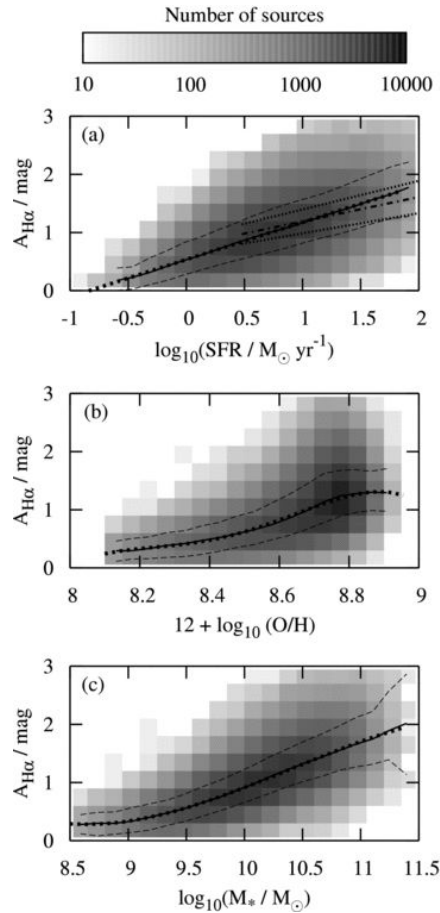


FIGURE 1.8: Correlation between H-alpha extinction with star formation rate (top); metallicity (middle); stellar mass (bottom) from a sample of 90,000 galaxies from the Data Release 7 of the Sloan Digital Sky Survey (Garn & Best 2010).

The overarching goal of this thesis is to compare these two specific traits, metallicity and dust content, in LSB galaxies to determine if they result from galactic overfeeding. Warm dust maps will be created by deconstructing Spitzer IRAC 3.6 and 4.5 μ m images using the Independent Component Analysis (ICA) to separate the light from old stellar populations versus emission contributed by contaminants, including warm dust. This technique was developed by Meidt et al. (2012) and will be applied to our sample of 10 galaxies. Eventually, the warm dust maps from this thesis will be converted to include the content of cold dust. These dust maps will be compared with the metallicity content of LSB galaxies, which will be measured using the Visible Integral-field Replicable Unit Spectrograph - Prototype (VIRUS-P). A diagram showing the purpose and process of this project is seen in **Figure 1.9**:

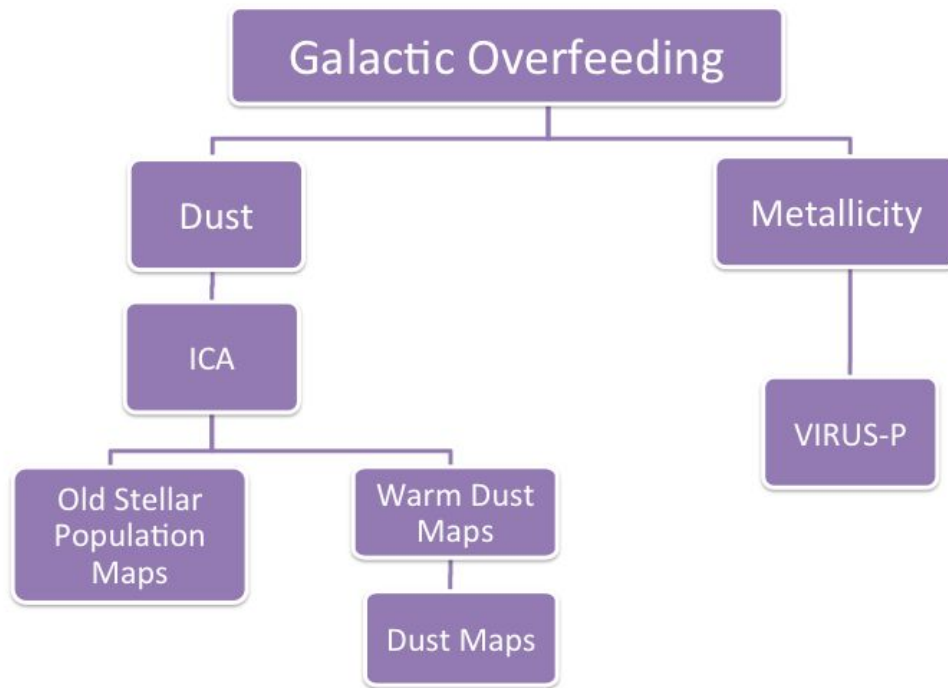


FIGURE 1.9: Diagram of the overarching goal of this project (this thesis).

This thesis consists of four additional chapters. Chapter 2 provides an overview of the historical background of LSB galaxies and their distinct characteristics, and significance of LSB

galaxies. Chapter 3 focuses on our selection of LSB galaxies, the ICA, and our procedure to apply it to our sample galaxies. Chapter 4 shows the results of implementing this technique and provides an analysis for each of the galaxies. Chapter 5 discuss trends in our results, possible refinements to our method, and insights into potential future work.

Chapter 2: Background

2.1 The First LSB Galaxy: Malin 1

The first low surface brightness (LSB) galaxy was discovered by accident, which shows how difficult they are to detect. The story begins in early 1984. The Las Campanas Photographic Survey of the Virgo Cluster, conducted by one of the most influential astronomers in the 20th century, Allan Sandage and his collaborators, revealed that there were many dwarf galaxies that were extremely diffuse. For a diffuse object to be in a galaxy cluster was an intriguing scenario because high gas density should ignite star formation. That same year, Ellis et al. (1984) also discovered more diffuse objects in the field. Was it possible that these objects were common but not yet discovered? Greg Bothun and Chris Impey wanted to explore this question further to see if any LSB galaxies were missed in Sandage's survey.

They collaborated with Australian astronomer, David Malin, who created and mastered a method of photographic amplification to bring out low contrast features. Malin used this method on selected one-square-degree areas to see if anything could be found. Surprisingly, the results showed strong evidence of small diffuse objects. Many of their colleagues were skeptical of the data, proposing that they could be artifacts of processing, water spots, or specks of dust (Bothun et al. 1997). In 1985 and early 1986, the smudge galaxies were further imaged using the Las Campanas 100-inch Telescope. The results confirmed that these objects were indeed real, though all but one lacked structure: "This object appeared to have a faint spiral structure that was connected to a point-like nuclear region" (Bothun et al. 1997). Using the Palomar 200-inch Telescope in California, Jeremy Mould and Bothun acquired an optical spectra of this nucleus, which showed emission lines at a recessional velocity of $\sim 25,000 \text{ km sec}^{-1}$. The Virgo Cluster

has a recessional velocity of only $1,150 \text{ km sec}^{-1}$, which meant that this object was farther away than the Virgo Cluster (Bothun et al. 1997). On October 21, 1986, more observations were made at the Arecibo Observatory, using the 21-cm wavelength line of neutral hydrogen (HI) gas. HI is a good measurement of a galaxy's velocity since hydrogen radiation is not affected by interstellar dust and can be detected anywhere in the spiral galaxy. Results revealed a "double horned" profile, revealing that the object was a rotating disk galaxy. It became the first LSB galaxy to be discovered, and was named Malin 1, after the process that helped uncover it.



FIGURE 2.1: Malin 1 (Galaz et al. 2015).

There are several reasons why it took so long to find Malin 1. We know today that it is located 1.19 billion light years (336 Mpc) away in the Coma Berenices constellation, near the North Galactic Pole. It is one of the largest spiral galaxies ever discovered, with a diameter of 650,000 light years (20,000 pc), 6.5 times the diameter of our Milky Way! Its apparent brightness is 15.80, which is quite faint (for reference, the naked eye can see stars up to a magnitude of 6.5). Because of the combination of its huge size, diffuseness, and low star formation rate, Malin 1 was very difficult to detect. Today, LSB galaxies are discovered using

radio telescopes and through deep surveys, which require long exposures. The LSB galaxies explored in this thesis came from a deep survey imaged through the Spitzer Space Telescope (SST), which is discussed further in Chapter 3. To constitute which galaxies are considered an LSB galaxy, we need a threshold. In order to do that, the term “brightness” must be quantified.

2.2 Measurements of Brightness

Because the concept of brightness is arbitrary, how can an LSB galaxy be defined? The answer requires an understanding of how brightness is measured. Brightness in stars is measured in terms of the unitless, logarithmic scale of **magnitude**, of which, there are two types: apparent magnitude and absolute magnitude. Apparent magnitude (m) is the brightness of an object as it appears to an observer here on Earth. Absolute magnitude (M) is the intrinsic brightness of an object at a standard distance of 10 parsecs (32.6 light years). Historically, magnitude values are reversed: a negative magnitude value is brighter than a positive magnitude value. For reference, the Sun has an apparent magnitude of -26.74 and an absolute magnitude of 4.83. The difference between the two magnitudes provide a measurement of the object’s distance, as supported by the distance modulus, where d is in the distance measured in parsecs:

$$m - M = 5 \log(d) - 5 .$$

Light can also be measured in terms of energy. Stars are often modeled using a blackbody, an opaque object that absorbs all light and emits thermal radiation. The energy per unit area radiated from a star is called flux (F). This quantity is highly dependent on the temperature T , as summarized in the Stefan-Boltzmann Law, where $\sigma = 5.67 \times 10^{-8} [W/M^2K^4]$:

$$Flux = \sigma T^4 [W/M^2] .$$

Units of flux are given in watts/meters² [W/M^2]. The hotter the star, the higher the flux.

To find the **luminosity**, or the total energy radiated in all directions from a star's radius (r), the flux and the surface area are multiplied:

$$Luminosity = 4\pi r^2 \sigma T^4 [W].$$

Luminosity is an intrinsic property of the star and does not vary with distance. Units of luminosity are given in watts [W] or in terms of the luminosity of the Sun, $L_{\odot} = 3.846 \times 10^{26} W$. Stars with large luminosities must be either very hot or very big.

Because a galaxy contains many stars and is spatially expanded, its brightness is measured by the space density of stars per square arcsecond in the sky. This logarithmic quantity is called **surface brightness** (μ) and is measured by the flux (F) divided by the solid angle Ω subtended by the source:

$$surface\ brightness, \mu = \frac{dF}{d\Omega} [magnitude/arcseconds^2].$$

The concept for surface brightness can also be summarized as follows: if a galaxy has a surface brightness of 20 mag arcsec⁻², then if the galaxy is divided into squares with one arcsecond on each side ($\approx 1/3600^\circ$), on average, one square will emit the same amount of light as a 20th magnitude star. As supported by the equation, surface brightness is independent of distance. Although an object is fainter with distance, it is correspondingly smaller in the visual area.

It can be difficult to determine when a galaxy ends. Because galaxies do not have uniform surface brightness, the brightest part at the center (μ_0) is often used to determine the object's visibility. A high surface brightness value generally implies that the galaxy is diffuse and a low surface brightness (LSB) galaxy. A low surface brightness value implies that the galaxy is compact and is a high surface brightness (HSB) galaxy. Several researchers have

different values to what constitutes the brightness threshold of an LSB galaxy (e.g., Chung et al. 2002 and McGaugh 1994 sets this value to $\mu_0(B) > 23$; Adami et al. 2006 sets this value to $\mu_0(R) > 24$). In this thesis, this threshold value is set to $22 \text{ mag arcsec}^{-2}$; any galaxies that have a low surface brightness value greater than $22 \text{ mag arcsec}^{-2}$ will be considered a LSB galaxy.

2.3 Features of LSB Galaxies in Sample

Besides having a surface brightness that is greater than $22 \text{ mag arcsec}^{-2}$, LSB galaxies also vary in morphology. To narrow our sample, we selected galaxies that have these four features that we will discuss in this section.

2.3.1 Spiral Galaxies

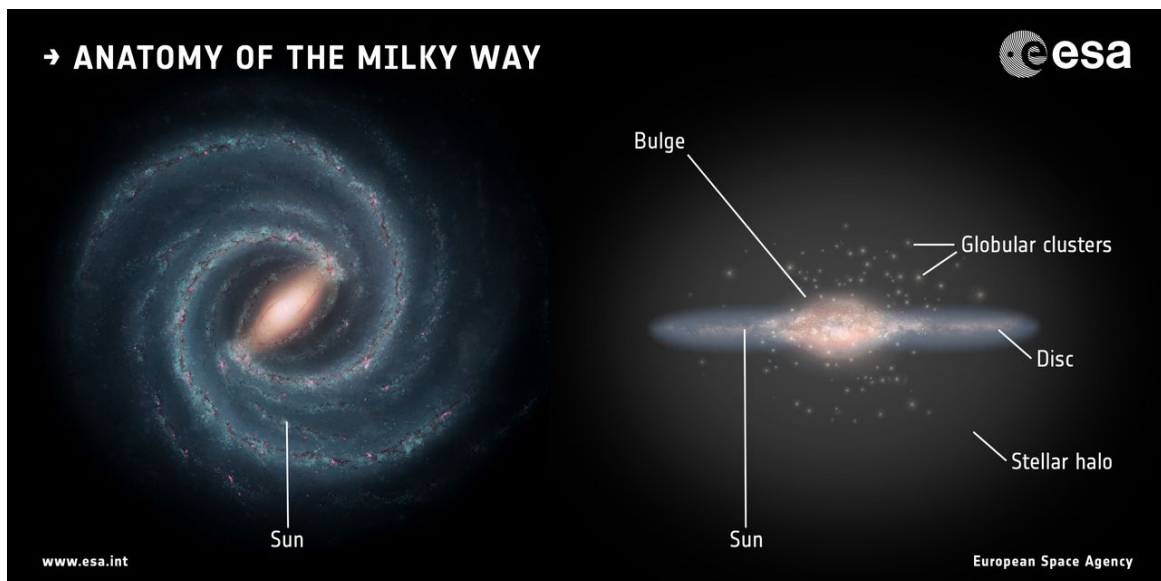


FIGURE 2.2: Anatomy of Milky Way (NASA/JPL-Caltech 2016).

All the LSB galaxies in our sample are spiral galaxies, which are the most observed galaxies in the universe – making up $\sim 77\%$ of documented galaxies (Sloan Digital Sky Survey)!

Figure 2.2 shows the different characteristics of a spiral galaxy. At the core of the galaxy is a

central bulge that contains mainly older, redder stars. Not all spiral galaxies have a bulge. This bulge is surrounded by a flat, rotating disk of young stars and interstellar matter. A near-spherical halo of globular clusters and dark matter encloses the galaxy. Some spirals also contain supermassive black holes in their cores. As seen in **Figure 1.1**, spiral galaxies are divided into two categories: normal spirals and barred spirals. Barred galaxies have a central bar-shaped structure composed of stars that normal galaxies lack. Our Milky Way is an example of a barred spiral galaxy. Spiral galaxies are further classified by how tightly their spiral arms are bound.

2.3.2 Blue Colored

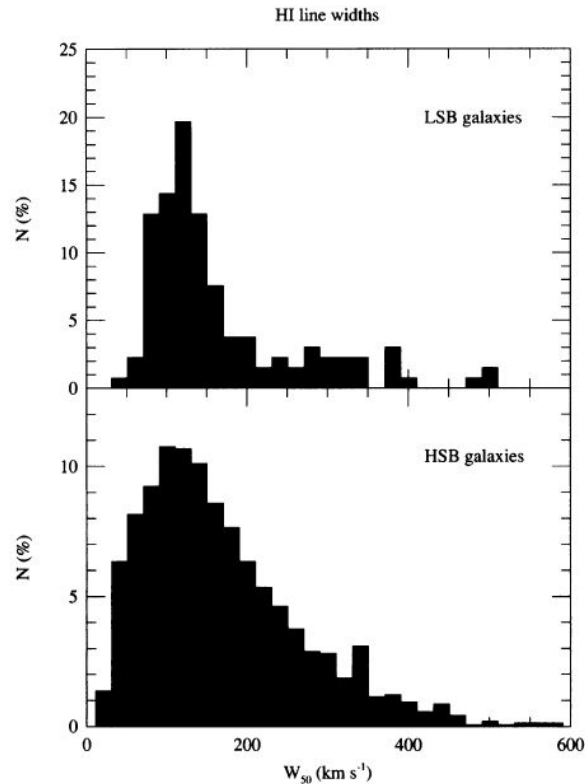


FIGURE 2.3: Fractional distributions of 21-cm velocity widths for samples of LSB and HSB galaxies. A galaxy that has a higher velocity is more massive. LSB galaxies have the same mass as HSB galaxies (Bothun et al. 1997).

The diverse phenomena in LSBs are categorized into various types: dwarf, giant, Red, and Blue LSB galaxies. Dwarf LSB galaxies are the most common type, so for a long time, there was a widespread notion that all LSB galaxies were dwarf galaxies or smaller in size. We know today that this notion is not true. **Figure 2.3** shows the distributions of 21-cm velocity widths for a sample of 131 LSBs from the Schombert et al. (1992) catalog and 1,500 HSBs from different sources of literature (Bothun et al. 1997). A galaxy that has a higher velocity implies that there is more mass. In this plot, LSB galaxies have similar sizes and masses to their high surface brightness (HSB) galaxy counterparts. A small percentage of LSBs are a Giant LSB or massive in size, such as Malin 1. These galaxies are typically found to be isolated and rarely interact with other systems (Das 2013).

A red LSB galaxy is a faded remnant that can no longer form stars because they were stripped of their gas in a process called Ram Pressure Stripping (RPS). This process occurs as galaxies move through the intracluster medium (ICM), wherein hot ICM gas strips away the galaxy. A galaxy that goes through RPS before it forms a substantial amount of stars will end up without enough gas to form more stars. Such galaxies appear red in color because red stars are old, lower-mass and cooler, while blue stars are young, massive, and hot. Blue LSB galaxies are gas-rich, are on the same mass class as the Milky Way, and are typically found in isolated areas. These blue galaxies will be the focus of this thesis because their evolutionary path still presents a puzzling mystery.

2.3.2 Dark Matter-Dominated

As mentioned in Chapter 1, all LSB galaxies are heavily dark matter-dominated. This was supported by their rotation curves and a higher mass-to-light ratio (de Blok and McGaugh

1996; McGaugh research website). In LSB galaxies, dark matter is concentrated at the core, which could explain their alternative evolutionary path. Our current understanding of dark matter is still limited, so there can only be speculations on the nature of dark matter.

2.3.3 Low Star Formation Rate

LSBs have all the gas to form stars, but their star formation rate remains low, at least an order of magnitude lower than in similar disk galaxies (Bothun et al. 1997). Bothun et. al (1997) argued that these systems lack two structural features that could cause low nuclear activity: bulge and bars. While this might have been true at the time the paper was written, some LSB galaxies have been found to have these features, such as UGC 628, disproving this argument.

2.3.4 Low Metallicity

As confirmed by the observations of McGaugh (1992), LSBs have low-metallicity. Astronomers use the term metallicity (Z) to describe the fraction of mass of an astronomical object that is found in elements heavier than hydrogen (X) or helium (Y), such as oxygen, silicon, and iron. Although many chemists would argue and highly disagree that these elements are non-metal, this term was used for convenience because most of the physical matter in the universe is in the form of these two elements. As a galaxy ages, its temperature increases until it is able to convert hydrogen and helium into heavier elements because it is high in metallicity. LSB galaxies are low in metallicity, implying that these galaxies could be in the early stages of their formation and have not been chemically enriched. Another explanation for the low metallicity in LSBs might be dilution of Interstellar Medium (ISM) in an older galaxy with inflowing intergalactic gas.

In summary, the LSB galaxies studied in this thesis have a surface brightness that is greater than $22 \text{ mag arcsec}^{-2}$, are blue in color, dominated by dark matter, have a low star formation rate, and are low in metallicity. This combination produces an outcome that questions our current understanding of galaxy evolution.

2.4 Significance of Low Surface Brightness Galaxies

Studying LSB galaxies represents an alternative path of galaxy formation that differs from the classical Hubble sequence. As seen in Chapter 1, there is no consensus on the specifics of this path. Because our understanding of how galaxies form and evolve is incomplete, learning more about LSB galaxies is a step towards closing that gap.

2.4.1 Quiescent Evolution

LSB galaxies are unevolved galaxies that form at a slower rate than their high surface brightness (HSB) galaxy counterparts. Their current star formation rate (SFR) is $\sim 0.1 M_{\odot} \text{yr}^{-1}$, compared with high surface brightness (HSB) Sc galaxies that have a star formation rate one magnitude higher, $\sim 4 M_{\odot} \text{yr}^{-1}$ (Kennicutt 1983). Consequently, this difference in SFR is seen in the gas depletion time. A typical HSB galaxy will consume all of its gas reservoir in a few billion of years (Gyr), while a LSB galaxy requires tens of Gyrs (de Blok & McGaugh 1996). This opens a window into understanding the the physical processes that allows an LSB galaxy to hold onto its gas without producing more stars.

2.4.2 Dark Matter

All LSB galaxies are heavily dark matter-dominated, especially at smaller radii. With a dark matter halo concentrated at the core – structurally different from high surface brightness

(HSB) galaxies – this raises the possibility that dark matter can play a part in the past and current star formation rate in LSB galaxies. Another possibility is that our current understanding of dark matter is incorrect. There is more dark matter content near the core of LSB galaxies, which may be easier to measure compared to HSB galaxies that have more dark matter content on the edge. The reasoning as to why there is more dark matter content in LSBs is not clear, which makes these galaxies wonderful laboratories to study dark matter and its role in galaxy formation and star formation process.

2.4.3 Missing Mass Problem

The measurement of the cosmic microwave background – electromagnetic radiation left over from the Big Bang – suggests that the Universe is made up of ~70% dark energy, ~23% dark matter, and ~4.6% of baryonic or ordinary matter (anything that contains protons and neutrons). Known as the “missing mass problem,” all the stars and galaxies make up only 10% of the predicted baryonic matter. So where can all this mass be hiding? Because LSB galaxies have high mass-to-light ratios, are dark matter-dominated, and are often overlooked, there is a possibility that some of this unaccounted mass is located in these galaxies. LSB galaxies account for a large fraction of the galaxies in the universe, ranging from 50% (Impey & Bothun 1997) to 10% (Hayward et al. 2005). Investigating LSB galaxies places better constraints on the fraction of LSB galaxies and provides a census of the distribution of baryons in the universe.

2.4.4 Star Formation Activity in Low Metallicity Environments

A characteristic of LSB galaxies is that they are all poor in metallicity. As discussed in Section 2.3.4, there are two explanations for this: LSB galaxies are in their early stages of formation and have not been chemically enriched, or LSB galaxies are older, but their interstellar

medium (ISM) have been diluted by inflowing intergalactic gas. The low metallicity of LSB galaxies makes them great candidates to study the effects of low metallicity on a star. This topic is rarely studied because it is hard to find examples of nearby galaxies that are metal poor. There are speculations that many processes relating to star formation, such as gas cooling, are not as efficient in a low metallicity environment. Analyzing the star formation rate in LSB galaxies provides us an opportunity to test these speculations.

Chapter 3: Materials and Methodology

3.1 Infrared

Different wavelengths can reveal varying stories about celestial objects. In the visible spectrum (390 - 700 nm), our view of the universe is obscured by interstellar dust, which is the light that is emitted by an object blocked by intervening dust particles. In the infrared (700 - 1×10^6 nm), which has wavelengths much longer than the visible, this problem is reduced because infrared light can pass through dust clouds without being as affected by it. The infrared spectrum is divided into three subsections: near-infrared, mid-infrared, and far-infrared. The boundaries between these three sections are not universally agreed upon. Infrared spectroscopy has become an important branch of astronomy, allowing astronomers to study the composition and structure of objects that are hidden in the optical.

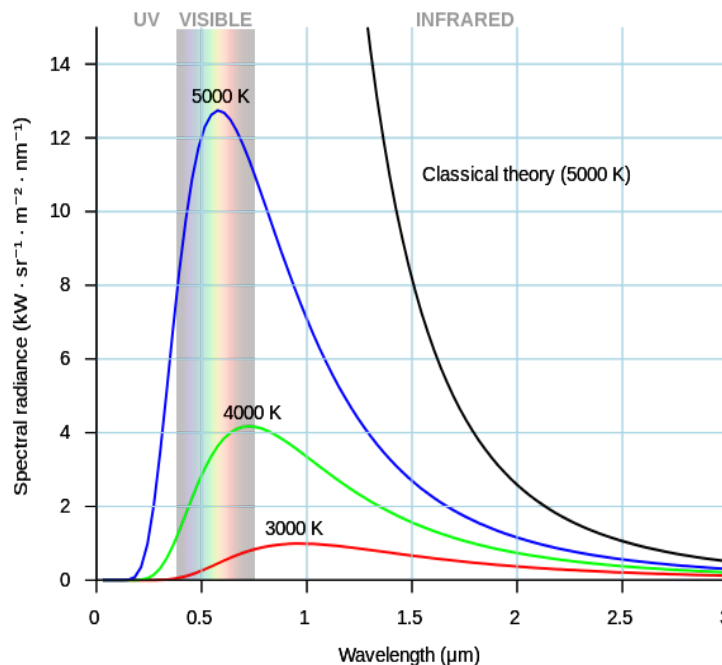


FIGURE 3.1: Black body curve. As the temperature of an object increases, the peak of the black-body radiation curves moves to higher intensities and shorter wavelengths.

All celestial objects emit infrared radiation. According to Planck's Law, the wavelength at which an object radiates its peak intensity is dependent on temperature (**Figure 3.1**). In general, the cooler the temperature, the more intense the object will be at farther infrared wavelengths. Therefore, different wavelengths in the infrared are effectively used to detect specific objects.

The near-infrared (0.7 - 5 μ m) can allow detection of cooler red stars and red giants, which are dying stars in their last stages of evolution. Because these stars, specifically K and M-type giants, dominate the stellar flux, the near-infrared is seen as an optimal window into detecting the older stellar population that makes up a large portion of the baryonic mass in galaxies and holds the fossil record of galaxy formation that has led to its current state. This energy range also samples dust and Polycyclic Aromatic Hydrocarbon (PAH) emissions, which will be discussed in Section 3.3. Because both dust and PAHs are formed from metals, the metallicity content at this wavelength can be estimated. Therefore, the near-infrared is the ideal bandwidth to reach the goals of this study: images at these wavelengths can be used to create dust maps to measure the dust content of the galaxy and create mass maps to show the distribution of mass within the galaxy.

3.2 Spitzer Space Telescope

Ground-based infrared telescopes are difficult to utilize because the water in Earth's atmosphere absorbs infrared radiation and also emits at infrared wavelengths. To overcome this problem, infrared telescopes are placed at high elevations in dry places, such as Antarctica, or in space. The Spitzer Space Telescope (SST) is one of many space infrared telescopes and is the

source for all data in this thesis (**Figure 3.2**). Spitzer was launched in 2003 and was the fourth and last of the NASA Great Observatories Program, each of which examined a specific wavelength of the electromagnetic spectrum: the visible light Hubble Space Telescope, Compton Gamma-Ray Observatory, and the Chandra X-Ray Observatory. Spitzer's primary mirror is 85 cm (33") in diameter and carries three instruments on board: Infrared Array Camera (IRAC), Infrared Spectrograph (IRS), and Multiband Imaging Photometer for Spitzer (MIPS).

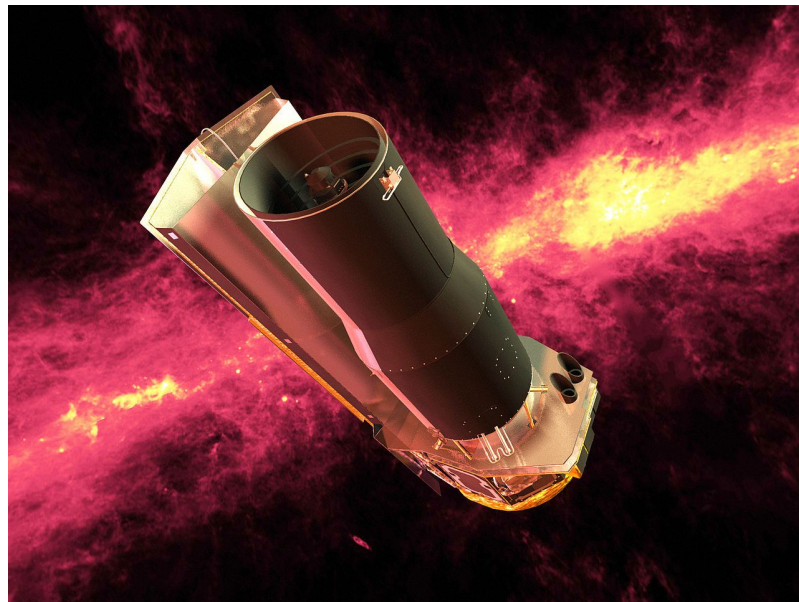


FIGURE 3.2 : Artist's conception of Spitzer Telescope (NASA/JPL-Caltech/R. Hurt 2005).

Although Spitzer has already far surpassed its life expectancy of 2.5 years, the telescope has faced many challenges. In 2009, Spitzer ran out of liquid helium, which is used as a coolant. Thus began the “warm Spitzer” mission. With the inability to cool the instruments, many of the tools became unusable. The telescope became bright in the infrared and it was hard to conduct further observations at any wavelengths longer than $5\mu\text{m}$. The two shortest wavelengths of the IRAC camera, $3.6\mu\text{m}$ and $4.5\mu\text{m}$, are the only channels that are still operable. It is predicted that Spitzer will last until the end of this decade.

3.3 Contaminants

All images used in this thesis are from the warm phases of Spitzer and can be found online in the Infrared Science Archive (IRSA). Although it is expected that old stars, M and K giants, contribute the most flux at 3.6 and the 4.5 μm , other additional features are also introduced in this bandwidth. This creates an inaccurate calculation of the integrated flux and mass. This section gives an overview of these different contaminants and why it is important to eliminate them in order to create accurate mass maps.

3.3.1 Polycyclic Aromatic Hydrocarbon

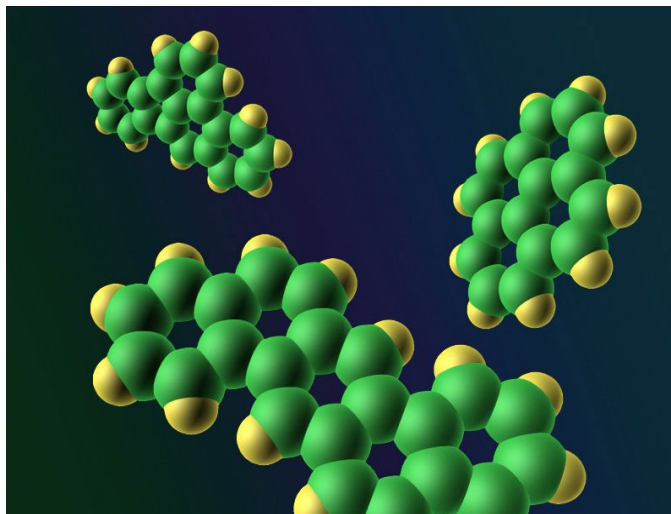


FIGURE 3.3: Polycyclic Aromatic Hydrocarbon (NASA/JPL-Caltech/R. Hurt 2005).

Polycyclic Aromatic Hydrocarbon (PAH) can be quite a mouthful, but by breaking these three words apart, this term can be explained. “Hydrocarbon” refers to a compound only consisting of carbon and hydrogen atoms. “Polycyclic” implies that these molecules have several loops of carbon atoms. “Aromatic” means that there is a strong chemical bond between carbon atoms. A visual representation of PAHs is given in **Figure 3.3**. These organic compounds are produced naturally here on Earth. When trash, oil, coal, or wood are burned, PAHs are released

in the air; when meat is grilled, PAHs are formed on the meat; when a cigarette is lit, PAHs are found in the smoke.

PAHs are quite abundant in space and are found in regions forming new stars, making them useful indicators of active star formation. Because PAHs are present here on Earth, their detection provides clues to the possible chemicals needed for life in the universe. After a PAH molecule is energized by absorbing photons of light, it re-emits this light at a lower energy. This process is called “fluorescence” and is most apparent in the infrared (Hurt 2005). The 3.3 μm PAH feature is present in the 3.6 μm band and the PAH continuum is featured in the 4.5 μm (Flagey et al. 2006).

3.3.2 Warm Dust

Dust is formed in stars and is released into the interstellar medium through explosions of dying stars (supernovae) or carried through a slow wind. The dust is recycled by the interstellar gas and is a vital ingredient for the formation of new stars. Dust particles are irregularly shaped and are extremely small, only a few molecules to 0.1 μm in size. They are composed of silicates, carbon, ice, and/or iron compounds.

The universe is filled with interstellar dust, which was once considered a nuisance to astronomers because it obstructs light in the visible and in the ultraviolet light. We have since learned the important roles that dust plays in different astrophysical processes. Because hot dust appears in the infrared, it contributes to some of emission: “Younger (hotter) stars are not expected to contribute significantly to the observed stellar emission. However, due to their strong UV fluxes, these younger stars can heat their surrounding dust, which, in turn, re-radiates at

longer wavelengths and can also account for a significant fraction of the light at 3.6 μm (Meidt et al. 2012)” (Querejeta et al. 2015).

3.3.3 AGB and RSG Stars

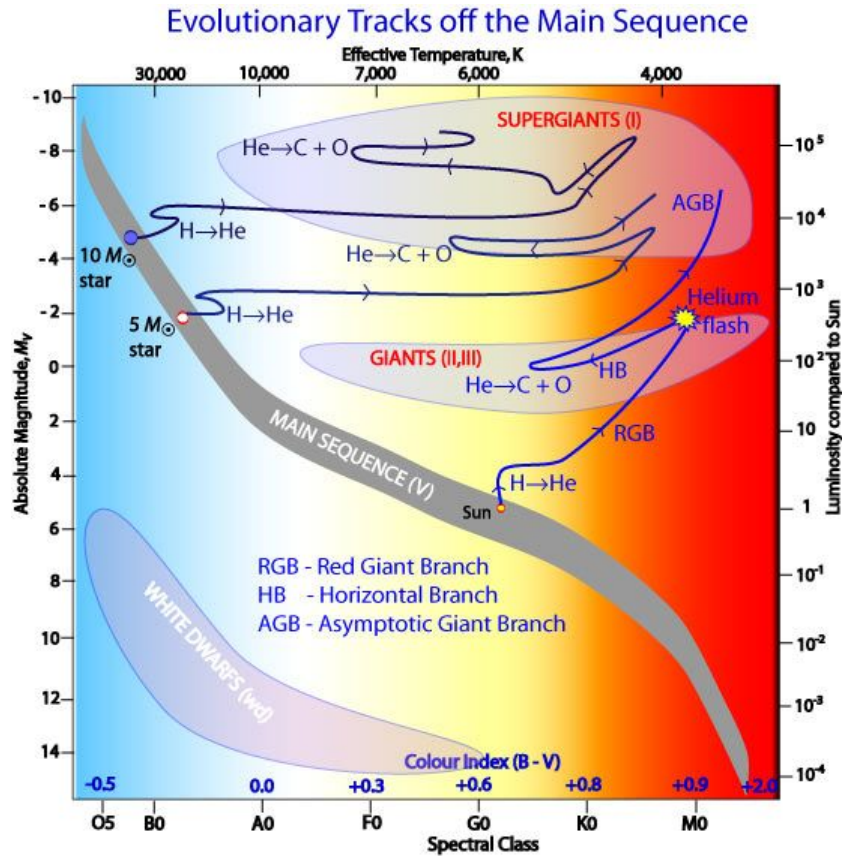


FIGURE 3.4: Evolutionary tracks of stars (Australia Telescope National Facility).

Mass is the biggest factor determining how a star will evolve throughout its lifetime. A high mass star will live a shorter life; a low mass star will live longer. As seen in **Figure 3.4**, the last phase for stars that have a birth mass range of 0.6-10 M_{\odot} will be an evolved, cooled luminous star in the Asymptotic Giant Branch (AGB). In this phase, the stars are thousands of more times luminous than the Sun due to burning of the hydrogen and helium shell. AGB stars appear very similar to red giants.

More massive stars that have a birth mass range of $11-30M_{\odot}$ will become red supergiants (RSG). These stars exhaust their hydrogen at a much faster rate. At this phase, helium is in their core and hydrogen is undergoing nuclear fusion in the outer shells, causing their stars to expand in volume. Because of this, RSGs are the largest stars in the universe. Both types of stars appear like “red knots” in a galaxy. The next section, further discusses a technique that identifies these types of stars as a contaminant in the $3.6\mu\text{m}$ image.

The content of these three sources varies from galaxy to galaxy and does not have much of an effect in total mass estimates. However, in one and two-dimensional representations of the mass estimated from an $3.6\mu\text{m}$ image, contaminants have a great effect on the results, potentially leading to overestimation in stellar mass maps (Meidt et al. 2012). Obtaining and producing unbiased mass maps are critical to understand the distribution of baryons and the underlying physics that has shaped that galaxy. Mass maps have been used in many studies, such as investigating torques exerted by the stellar structure (e.g., Zaritsky & Lo 1986; Foyle et al. 2010), studying the role of bars (e.g., Scoville et al. 1988, Knapen et al. 1995; Salo et al. 2010), and studying the spiral structure (e.g., Elmegreen & Elmegreen 1984; Elmegreen et al. 1989); Regan & Elmegreen 1997).

3.4 Independent Component Analysis

Though several techniques have been created to eliminate contaminants in IRAC images, they were not created for use as mass maps (Kendall et al. 2008; Hunter et al. 2006; Bolatto et al. 2007; de Blok et al. 2008). Some procedures require large uncertainties and some cannot be applied to a wide range of galaxies. Meidt et al. (2012) created a pipeline that separates light

from old stars and emission contributed by contaminants using the 3.6 and 4.5 μ m images. The method was first applied to six galaxies taken for the Spitzer Survey of Stellar Structure in Galaxies (S⁴G), a survey conducted by Spitzer with the goal of improving our understanding in the evolution and formation of nearby galaxies. The technique was later expanded by Querejeta et al. (2015), who applied the same method to the rest of the sample galaxies in S⁴G. The resultant images of the stellar flux of old stars are easily converted to reliable mass maps.

Independent Component Analysis (ICA) is a powerful technique that decomposes a multivariate signal into source signals. It assumes that the source signals are independent and less-gaussian. ICA is a widely used method of blind source separation (BSS), which distinguishes “blind” source signals from known mix signals. Although ICA is very similar to the Principal Component Analysis (PCA), PCA cannot identify source signals because it uses only the covariance, which does not provide enough information.

A common application used to explain the ICA is the “cocktail party problem,” in which two microphones are stationed in different locations of the room. These microphones record the signal, $x_1(t)$ and $x_2(t)$, with x_1 and x_2 being the amplitude and t being the time index. Two friends who are the sources of the signal, s_1 and s_2 , decide to speak simultaneously. If both speakers are in different parts of the room, the two microphones will record signals that contain different combinations of their voices. This combination can be expressed as a linear equation:

$$\begin{aligned} a_{11} \cdot s_1(t) + a_{12} \cdot s_2(t) &= x_1(t) \\ a_{21} \cdot s_1(t) + a_{22} \cdot s_2(t) &= x_2(t), \end{aligned}$$

where a_{11} , a_{12} , a_{21} , a_{22} are parameters that reflect the distances of the speaker to each respective microphones. The above equation can be expressed in vector-matrix notation as:

$$A \cdot s = x,$$

where A is the mixing square matrix, s is the source, and x is the source signal. The goal of ICA is to estimate A and recover each original source, s_i , which in this case, are the two voices. If the parameters a_{ij} are known, the linear equation is easily solved by multiplying both sides of $A \cdot s = x$ by A^{-1} . In most cases, the mixing matrix A is unknown and the only information given is the observed data x .

Although this task seems impossible, but the statistical properties of the signals s_i can be used to estimate a_{ij} . The sources must be assumed to be statistically independent. Variables s_1 and s_2 are said to be independent if information on the value of s_1 does not give any information on the value of s_2 . This holds true in the “cocktail party problem,” because the voices of the two individuals are independent of each other. The second assumption is that the sources must have a distribution that is less-gaussian. According to the Central Limit Theorem (CLT), the average of many independent random variables will have a distribution that is closer to a gaussian or a normal distribution rather than the distribution of the variable alone.

If both these assumptions are satisfied, then the mixing matrix A and the sources can be solved (Comon 1994). We find an unmixing matrix W such that

$$y = Wx,$$

If the mixing matrix A is square and nonsingular, then:

$$W = A^{-1} \text{ and } s = y.$$

Re-writing those equations, we find a value of s that is as close to the independent sources as possible:

$$y = Wx = WAs \approx s.$$

This can be achieved by finding a value of W that maximizes the non-Gaussianity of $y = Wx = WAs$. Non-gaussianity sources are vital for solutions to ICA. If the sources are gaussian after mixing, according to the CLT, they will become more gaussian, making it impossible to recover the original sources.

ICA has been used in many fields such as signal processing, financial data, and analyzing documents. Here, we apply these examples to astronomical images. Using the 3.6 and 4.5 μ m images, ICA can be used to extract the two underlying sources, flux from old stellar population and contaminants. ICA successfully separates both these components because they have different color ranges, as supported in **Table 3.1** (Querejeta et al. 2015). Old stars (age $\tau \sim 2-12$ Gyr) have colors in the range $-0.2 < [3.6]-[4.5]_{\text{stars}} < 0$, whereas dust and PAH emission all correspond to $[3.6]-[4.5]_{\text{dust}} > 0$. Because color is both independent and non-gaussian, all assumptions of the sources are satisfied and the ICA can be applied.

Source	Typical [3.6]-[4.5] Range
Old stars ^a	-0.2-0
Diffuse dust	$\sim 0.2-0.7$
PAH Emission ^b	~ 0.3
Dust in HII regions ^c	~ 1.0

TABLE 3.1: Different sources in IRAC images and corresponding color ranges (Querejeta et al. 2015)

^a Willner et al. (2004), Pahre et al. (2004), Peletier et al. (2012) Meidt et al. (2014), Norris et al. 2015

^b Dominated by PAH emission. Approximate estimation based on Flagey et al. (2006)

^c Representative number based on Blain et al. (2003); it can either correspond to hot dust, e.g., in HII regions, or, in the most extreme case, to hot dust heated to large temperatures near an AGN

3.5 Procedure

Here, we discuss in detail how the ICA technique is applied to the IRAC images and implemented in steps. This procedure was modified using the work of Meidt et al. (2012) and Querejeta et al. (2015).

Step 1: GATHER THE 3.6 AND 4.5 μ m IMAGES

Meidt et al. (2012) and Querejeta et al. (2015) successfully used ICA to extract the two sources from S⁴G images, which are publically available on <http://irsa.ipac.caltech.edu/data/SPITZER/S4G/>. Our list of target LSB galaxies, introduced in a later section, was not observed in the S⁴G. Images of the LSB galaxies in this thesis are taken from the Spitzer Heritage Archive, which provides access to all Spitzer data from the Cryogenic and Warm Mission eras. Its web-based interface can be accessed at:

<http://sha.ipac.caltech.edu/applications/Spitzer/SHA/>.

There are several individual search options on the website. The different level options, 0, 1, and 2, correspond to differences in image processing. Level 0 is the raw data that have not been processed. Level 1 or Basic Calibrated Data (BCD) are individual data frames that have been calibrated from the Spitzer pipeline. Level 2 or post-BCD (PBCD data) are the products of combining these individual data frames, also known as mosaics. In this thesis, only PBCD data were used.

After downloading the data, the zip file was unpacked and included three different types of images. The mosaic files, which end with “maic.fits” as the image’s filename, are used in this project. The other two files, uncertainties (“munc.fits”) and mosaic coverage (“mcof”), are coded by channel. The coverage file stipulates the number of frames for each position observed.

Both 3.6 μm (channel 1) and 4.5 μm (channel 2) mosaic images were needed to analyze the given galaxy.

Step 2: ALIGN AND CROP IMAGES

After the images are gathered, both sets of images need to be aligned and cropped. Ideally, each galaxy should be in the center of an image with some amount of background included. Even though this step seems very simple, it is highly important that the two images be aligned because even a small misalignment produces errors after ICA. Most of the images used had to be rotated into alignment because they did not come from the same set of observations. The position of each galaxy was located by comparing it with the RA and Dec of the galaxy listed on the astronomical database, SIMBAD (<http://simbad.u-strasbg.fr/simbad/>).

Step 3: CONVOLUTION KERNEL

Because the accuracy of the solutions may be influenced by small differences in the 3.6 and the 4.5 μm point-spread functions (PSF), both images were to be blurred to narrow the error. The convolution kernel is calculated by Aniano et al. (2011) to match the 3.6 and 4.5 μm images. Meidt et al. (2012) notes that the choice of kernel does not significantly impact the results, perhaps because the two bands have point spread functions of comparable sizes. But this step is necessary for selected cases, especially fields that have point sources that are bright or unsaturated. The code to complete this step was written in Python (**Appendix A**).

Step 4: BACKGROUND SUBTRACTION

Once each image was blurred, the background level was subtracted from both sets of images. The background level was determined by locating five rectangular regions of the background in the image and calculating a median value for each of them. The median is used to

eliminate outlier points to avoid including a star in the region. The background value was found by finding the average of the median value of the five regions. The background value was then subtracted from image. Note that it is possible to get a negative-valued pixel background subtraction. The code to complete this step was written in Python (**Appendix B**).

Step 5: HIGH SIGNAL TO NOISE THRESHOLD

ICA cannot accurately separate two sources if their average signal-to-noise (S/N) is too low. Signal-to-noise measures how much signal there is relative to the noise levels, determining how well an object was measured. We completed this step by determining the threshold visually. We ran each image through ICA so that the result included a majority of the galaxy with little background. For all images, this threshold was set to 0.0001.

Step 6: PRELIMINARY MASKING

Because the ICA technique maximizes the non-Gaussianity of the sources, it is extremely sensitive to outliers. This means that a few pixels with different colors can bias the whole result. Only the galaxy itself should be analyzed by ICA. To achieve this, an elliptical region file that includes the galaxy only was created. If a pixel fell within this region, it was analyzed by the ICA. Another region file was created to mask out field stars, background galaxies, and pixels that were too bright. If a pixel fell within these regions, it was ignored. Masking was done by eye. All region files were created in ds9.

Step 7: RUN IMAGE THROUGH THE ICA

The $3.6\mu\text{m}$ and $4.5\mu\text{m}$ images were input to ICA, where the images were decomposed to trace either the old stars or the containment sources of emission by maximizing the distinction in the [3.6]-[4.5] color of these two components. For this step, we utilized FastICA, which was

developed by Hyvärinen (1999) and Hyvärinen & Oka (2000). The algorithm and code used came from the IT++ Library and are publicly available at <http://itpp.sourceforge.net>. The initial guess of the mixing coefficients was set to possible values of the expected color range of stars and dust ($-0.2 < [3.6]-[4.5]_{\text{stars}} < 0$ and $0 < [3.6]-[4.5]_{\text{dust}} < 1.5$). Eventually, the ICA departs from these initial seeds and then converges to a final solution. After the two images have gone through the ICA, two vectors of the two sources are left. These vectors are then converted back into an image and saved as an FITS file. The x and y position of the pixel with respect to the input image was noted. The code to complete this step was written in C++ (**Appendix C**).

Step 8: ANALYZE IMAGES AND REPEAT STEPS 4-7 IF NECESSARY

The colors of the new images are compared to check if the image of the stellar flux is consistent within the expected range of M and K giants. This process may introduce observational artifacts, caused by the presence of a saturated nucleus or by a PSF mismatch around bright central sources. For such cases, those pixels are masked and steps 6-7 are repeated. The resulting image is of the old stellar light, free of contaminants such as dust and PAHs.

3.6 Replication and Comparison

The same procedure, as described in Section 3.5, was replicated on one of the galaxies in S⁴G, NGC 2976. The nucleus and a bright star that was in the frame were masked out. In the non-stellar image, the HII regions are apparent in both the upper and lower end of the galaxy. As seen in **Table 3.2**, our replication is consistent because the same structures and morphology are seen in the galaxy in both the stellar and non-stellar images of NGC 2976 produced by Querejeta et al. (2015). We are now ready to move on with our target galaxies.

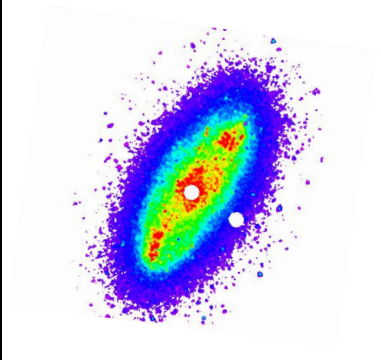
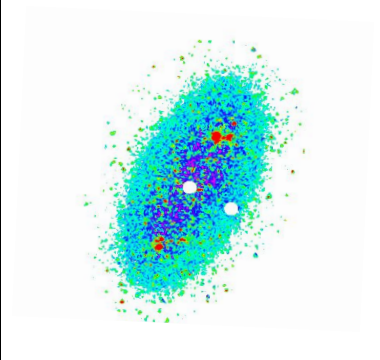
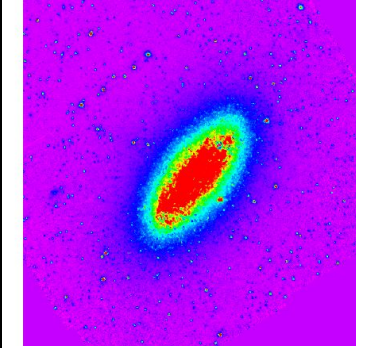
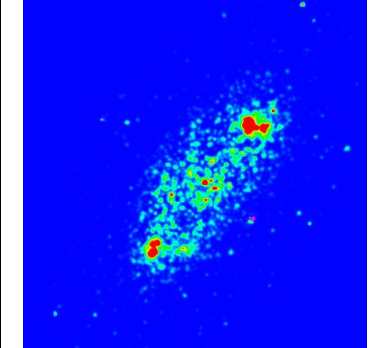
	Stellar	Non-stellar
Our method		
Querejeta et al. (2015)		

TABLE 3.2: Comparison of stellar and non-stellar images of NGC 2976 of our analysis (top) and Querejeta et al. 2015 (bottom).

3.7 Target Selection

There are a total of 10 low surface brightness (LSB) galaxies in our sample. These galaxies are part of the larger MUSCEL (MULTIWavelength observations of the Structure, Chemistry and Evolution of LSB galaxies) Program, which was created to constrain and understand the star formation history and the evolutionary path of LSB galaxies. This program was designed with three segments: archival Spitzer IRAC observations, ultraviolet (UV) observations and ground-based optical spectral. Archival Spitzer IRAC Observations are needed to constrain the integrated star-formation history. As previously stated, light in the infrared mainly traces the oldest stars. Galaxies that did not have images in both the 3.6 and 4.5 μ m were excluded. UV observations needed to constrain the current star formation rate were observed by

the Swift Ultraviolet and Optical Telescope. The ground-based optical spectra utilize emission line diagnostics to estimate the star formation rate, gas-phase metallicity, and metallicity gradient. The spectral observations were conducted on the Mitchell Spectrograph, commonly known as the Visible Integral-field Replicable Unit Spectrograph - Prototype (VIRUS-P), on the 2.7-m Harlan J. Smith Telescope at Mount Locke, TX. This was the upper limit for the size of the galaxy, because the galaxy needed to sit comfortably on the $1'7 \times 1'7$ field of view of VIRUS-P. The lower limit was that the galaxy needed to be close enough to see its details, given the effect of Earth's atmosphere and the faintness of the galaxy to begin with. In addition, galaxies that were edge-on in our line of sight ($i > 85^\circ$) were also avoided because their orientation decreased the galaxy coverage. The galaxies were first selected from the LSB galaxies cataloged in Kim (2007) and McGaugh & Bothun (1994) and were chosen based on the criteria stated above. **Table 3.3** summarizes our galaxy sample.

Galaxy	SIMBAD Label	Alt. ID	RA	Declination	Coordinates
UGC 628	<i>"Galaxy"</i>	LEDA 3639	01 00 52.05	+19 28 32.9	15.2163 +19.4758
UGC 731	<i>"Galaxy"</i>	LEDA 4202	01 10 44.00	+49 36 07.9	17.6829 +49.6022
UGC 11748	<i>"Galaxy in Group of Galaxies"</i>	LEDA 66791	21 27 39.734	+45 28 58.70	321.9158 +45.4830
UGC 11820	<i>"Low Surface Brightness Galaxy"</i>	LEDA 67421	21 49 28.64	+14 13 51.4	327.3683 +14.2311
UGC 1230	<i>"Low Surface Brightness Galaxy"</i>	LEDA 6451	01 45 32.251	+25 31 17.28	26.3854 +25.5211
F415-3	<i>"Low Surface Brightness Galaxy"</i>	LEDA 9705 UGC02017	02 32 45.24	+28 50 26.9	38.1852 +28.8393
F583-5	<i>"Low Surface Brightness Galaxy"</i>	LEDA 86661*	15 45 43.9*	+17 18 41*	236.434 +17.314
F584-2	<i>"Galaxy in Cluster of Galaxies"</i>	LEDA 56745 UGC 10140	16 01 49.703	+18 43 14.63	240.455 +18.721
UGC 5709	<i>"Galaxy"</i>	LEDA 31042	10 31 16.253	+19 22 58.71	157.8175 +19.3831
F563-V2	<i>"Low Surface Brightness Galaxy"</i>	LEDA 86666* ESDO 563-02	08 53 03.9*	+18 26 09*	133.2720 +18.4384

TABLE 3.3: List of sample galaxies

* corresponding coordinates are for starred name, mainly due to higher precision

Chapter 4: Results


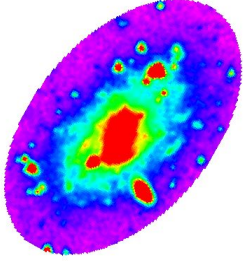
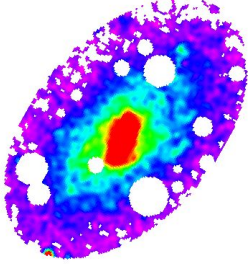
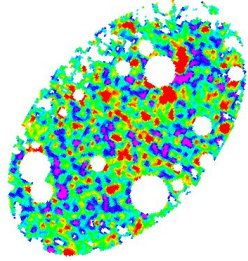
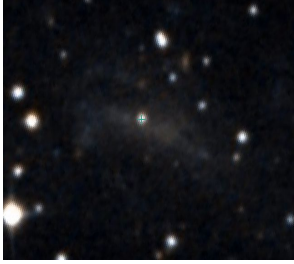
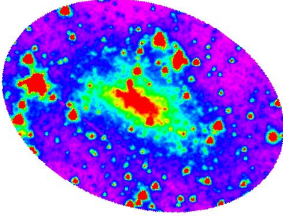
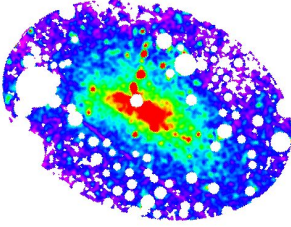
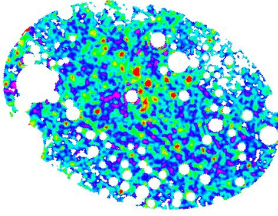
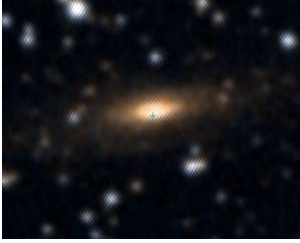
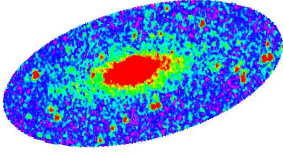
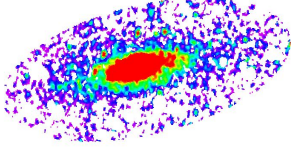
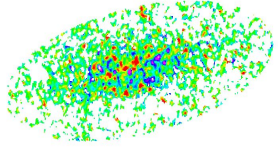
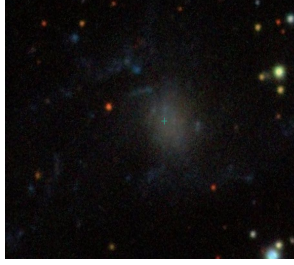
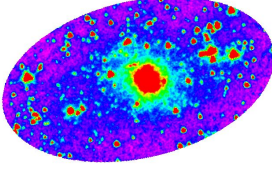
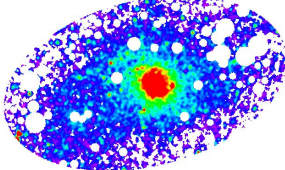
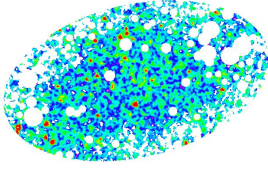
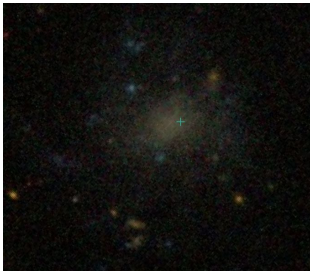
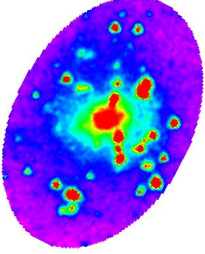
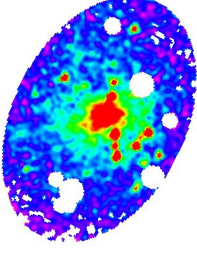
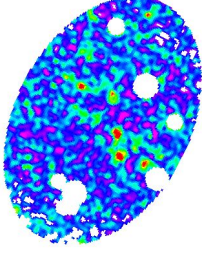
The procedure as described in Chapter 3 was replicated with our target LSB galaxies. The 3.6 μ m images, along with stellar and non-stellar images of each respective galaxy in our sample, are given in **Table 4.1**.

4.1 Analysis

As stated in Chapter 1, the goal of this project is to determine the dust and metallicity content of these target galaxies to access if low surface brightness (LSB) galaxy are the result of High Velocity Clouds weakening the metal content in gas. In this section, we analyze these two traits in each galaxy using the stellar and non-stellar images. There are four possible results when describing a region of the galaxy: presence of dust emissions and absence of an old stellar population, detection of both dust emissions and an old stellar population, absence of both dust emissions and old stellar population, and absence of dust emissions and the existence of an old stellar population. **Table 4.2** summarizes the potential causes for these outcomes.

	Dust emission / HII regions	No dust emission / No HII regions
Old stellar population	<ul style="list-style-type: none"> • High star formation rate. This is expected since dust is needed to form more stars 	<ul style="list-style-type: none"> • Dust has been dispersed throughout the galaxy • Young stars are not present so warm dust does not show up in the non-stellar image since there is nothing to heat up the dust
No old stellar population	<ul style="list-style-type: none"> • Region has been forming stars, but it has not yet built up enough stars to appear in the stellar image. • The region just began forming stars 	<ul style="list-style-type: none"> • No star formation activity. Low star formation rate could be due to the lack of dust that is present in the galaxy since dust is needed to form more stars

TABLE 4.2: Summary of explanation for different combinations of outcome

	SDSS/SDS	3.6 μ m	Stellar	Non-stellar
UGC 628				
UGC 731				
UGC 11748				
UGC 11820				
UGC 1230				

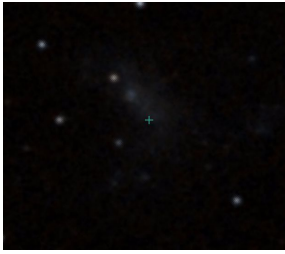
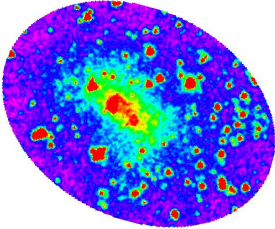
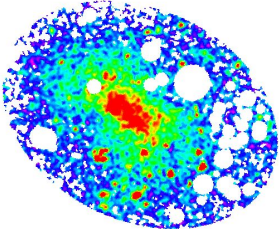
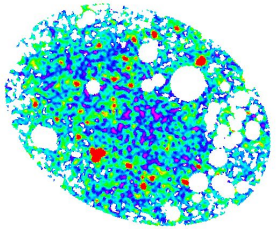
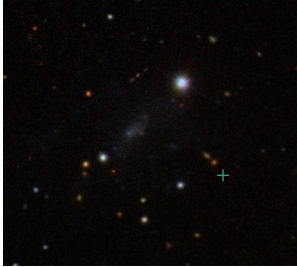
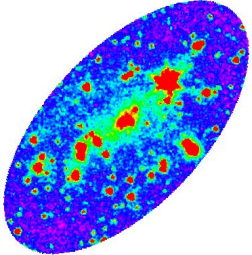
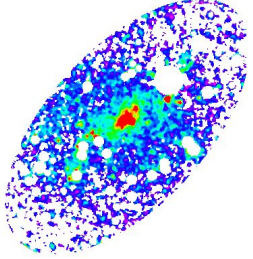
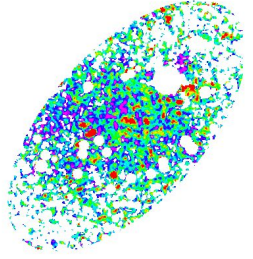
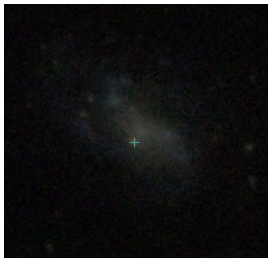
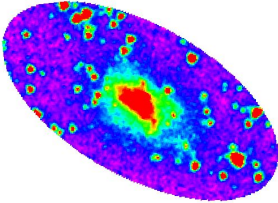
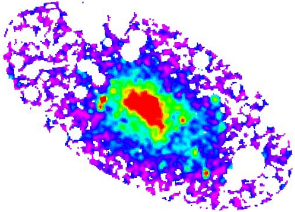
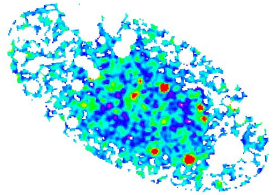

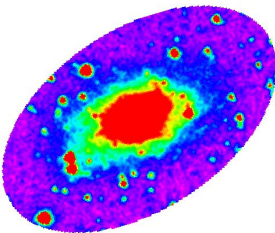
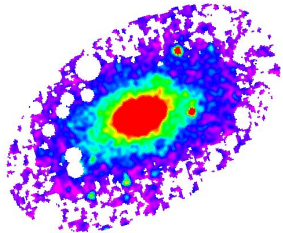
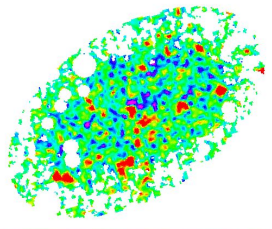
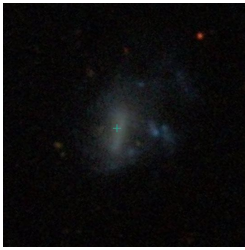
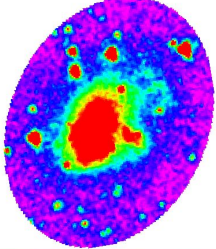
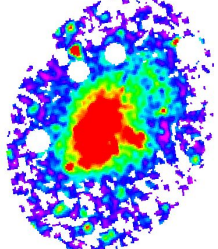
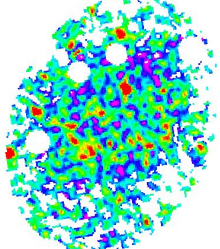
	SDSS/SDS	3.6 μ m	Stellar	Non-stellar
F415-3				
F583-5				
F584-2				
UGC 5709				
F563-V2				

TABLE 4.1: Comparing the 3.6 μ m image, stellar and non-stellar image of each galaxies in our sample

4.1.1 UGC 628

UGC 628 is an extreme late type galaxy, classified as a Magellanic Spiral (Sm) by de Vaucouleurs et al. (1991). Sm is the result of a transitional phase between a dwarf spiral galaxy and an irregular galaxy. This LSB galaxy has been studied extensively because it has a bar, which is rare for a LSB galaxy. Only 3-4% of sample LSB galaxies have a slow bar, whereas for high surface brightness (HSB) galaxies, this proportion is 30% (Mihos et al. 1997; Elmegreen et al. 1990).

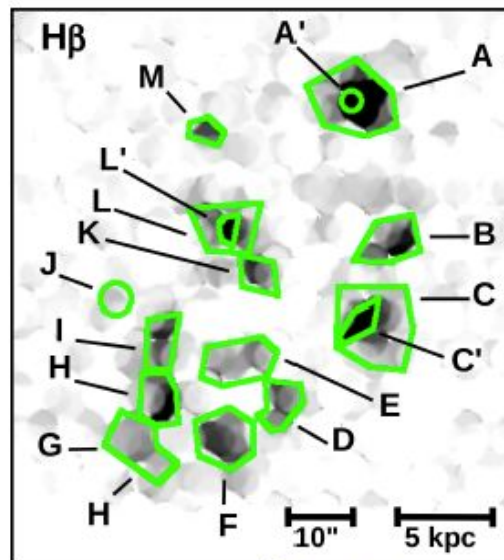


FIGURE 4.1: Different HII regions in UGC 628 labeled (Young et al. 2015).

In the 3.6 μ m image above, the bar is apparent in the central regions, with spiral arms branching off of it. There is one distinct region that is worth noting: region A is located on the upper right right side of the galaxy in **Figure 4.1**. This is a giant HII region that is seen in the non-stellar image, but not in the stellar image. This is surprising because it implies that the actively forming stars in these regions must be young because none were present in the stellar image. Region A accounts for a third of all the star formation in this galaxy and has a SFR of

$0.10 \pm 0.06 M_{\odot} \text{yr}^{-1}$ (Young et al. 2015). As supported by the images, the inner part of UGC 628 is relatively dust-free, implying that it lacks star formation. This is true as it has been this way for about 2 billion years (Young et al. 2017).

4.1.2 UGC 731

This is a “lopsided” galaxy that is diffuse and has a shapeless structure, as seen in the colored image in **Table 4.2**. Because the structures of UGC 731 is so faint and hard to see, this galaxy has been classified as an irregular galaxy (Im) by de Vaucouleurs et al. (1991). Im is a subtype that lacks spiral structures. There appears to be a nucleus in the galaxy, which was masked out for the ICA analysis. There are a few isolated clumps of HII regions that trail on the upper part of the galaxy and near the nucleus in both images. On the lower half of the galaxy, there are no HII regions, but there are a few areas of old stellar population. Because of the lack of dust emission it is possible that the lower part of the galaxy may no longer be forming stars, while the upper outer part of the galaxy is. The star formation rate of UGC 731 is $0.16 \pm 0.02 M_{\odot} \text{yr}^{-1}$ (Kim 2007).

4.1.3 UGC 11748

Classified as an S galaxy, this relatively large galaxy contains a big bulge in the center and has an inclination of 81° , which explains why the spiral arms are indistinguishable (Nilson 1973). UGC 11748 is a marginal LSB galaxy, meaning that it is on the boundary between a LSB galaxy and a HSB galaxy. Therefore, the star formation patterns in the galaxy were expected to be very similar to a HSB galaxy, with star formation activity near the center. This was confirmed because there is a mild level of activity in the center and relatively dust-free outer regions with

the lowest-level of dust emissions out of the ten samples. Many pixels are missing in the images due to the low signal-to-noise in the input images.

4.1.4 UGC 11820

This galaxy is classified as a Sm galaxy (de Vaucouleurs et al. 1991). UGC 11820 has amorphous structure with a central peak that is believed to not be a bulge. Its spiral arms are indistinguishable and very diffuse. There is one small prominent HII region on the bottom, outer part of the galaxy that appears in both sets of images. Overall, the galaxy has a moderate level of dust. Based on these observations, these characteristics imply that the galaxy is not actively forming any new stars. This conclusion is supported by Kim's (2007) calculation of the SFR, which is $0.07 \pm 0.04 M_{\odot} \text{ yr}^{-1}$.

4.1.5 UGC 1230

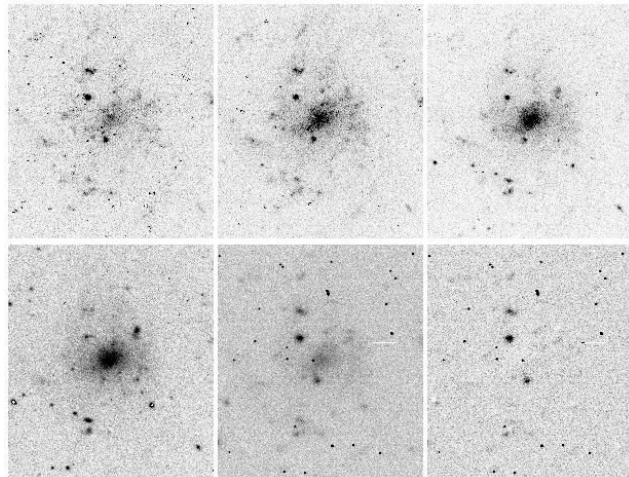


FIGURE 4.2: UGC 1230 taken in different wavelengths from left to right: U, B, V (top); I, H α , continuum subtracted H α (bottom) (McGaugh research website).

Classified as a Magellanic Spiral (Sm) galaxy, this face-on large galaxy has an extremely thin disk that is blue with diffuse spiral patterns (McGaugh et al. 1995). The spiral arms are very hard to see, but are more apparent in the bluer bands (**Figure 4.2**). There are a series of isolated

HII regions located at the lower and upper part of the galaxy that appear both in the stellar and non-stellar images. Because the spiral arms are hard to locate in the input images, it is possible that the HII regions are tracing the spiral arms. This would be expected because spiral arms contain many young, blue stars. However, if the HII regions are not tracing the spiral arms, this would show that there is sporadic star formation throughout the galaxy. Surprisingly, all active star formation is located in the outer part of the galaxy. The star formation rate for UGC 1230 is $12.3 \pm 1.3 M_{\odot} \text{ yr}^{-1}$ (Kim 2007), which is higher than those of the other sample LSB galaxies. Overall, the galaxy has a moderate level of dust.

4.1.6 F415-3

Classified as an irregular (Im) galaxy, F415-3 has a morphology that is lopsided and diffuse, similar to UGC 731 (de Vaucouleurs et al. 1991). There were lots of foreground stars in the field of view, that were masked. There is one HII complex in the contaminant image, near the lower left, outer part of the galaxy. Overall, there is no star formation activity in the center and the galaxy is fairly dust-free.

4.1.7 F583-5

Classified as an Sm galaxy, F583-5 is very diffuse and has indistinguishable spiral arms. It has a central peak, which could be a bar or bulge. There are several foreground stars in the field of view that were masked. Unlike the other LSB galaxies in our sample, the decomposed images of F583-5 show that a HII region near the center, implying that there is active star formation. In general, the galaxy is quiet and the dust emissions are at moderate levels.

4.1.8 F584-2

This galaxy is classified as an irregular galaxy (Im) and is very diffuse and faint. It has a distinct red region in the galaxy that can be seen in the color image. There are several HII regions located on the right part of the galaxy. Several of these regions appear in both images, suggesting that they are actively forming stars and have been for some time. There is one particular HII region in upper left part of the galaxy that stands out because it appears in the non-stellar image, but not in the stellar image. This region could be actively forming more stars in the recent past or perhaps has not built up enough stars to appear in the stellar image. Another interesting point about the contaminant image is the location of the HII regions: they are all isolated and dispersed in the outer regions, except for one near the center. The galaxy has a moderate level of dust emission.

4.1.9 UGC 5709

This is one of the reddest LSB galaxies in the sample, suggesting that it is mature. It is classified as a Sd galaxy and contains a nucleus in the center (de Vaucouleurs et al. 1991). Two distinct HII regions are located on the right side of the galaxy and upper part of the galaxy. Both of these regions appear in the stellar and non-stellar images, implying that it is actively forming stars. There are other isolated HII regions throughout the galaxy, suggesting sporadic star formation. Surprisingly, a low level of dust emission is observed, possibly due to the absence of young stars.

4.1.10 F563-V2

This galaxy has a distinct young star cluster located on the right side. In the non-stellar emission image, this region has weak HII regions. There is one visible HII region in the upper,

outer part of the galaxy that does not show up in the stellar image, which could mean that it just began forming stars. In general, the galaxy has a low dust emission and a low star formation.

Chapter 5: Conclusion and Discussion

The goal of this thesis is to construct warm dust maps, which will eventually be used to compare with the metallicity of low surface brightness (LSB) galaxies. These two traits, metallicity and dust content, can be used to determine if the evolutionary path of LSB galaxies is the result of galactic overfeeding, receiving more gas than they can consume. To calculate dust contents, we have replicated and applied Independent Component Analysis (ICA) to Spitzer IRAC 3.6 and 4.5 μm images on 10 LSB galaxies: UGC 628, UGC 731, UGC 11748, UGC 11820, UGC 1230, F415-3, F583-5, F584-2, UGC 5709, F563-V2. These images were decomposed to trace either the old stellar population or the contaminant sources of emission, which included Polycyclic Aromatic Hydrocarbons (PAHs), warm dust, intermediate-age asymptotic giant branch (AGB) stars and red supergiant (RSG) stars. ICA separates both these two components because they have different color ranges. Old stars (age $\tau \sim 2\text{-}12$ Gyr) have colors in the range of $-0.2 < [3.6] - [4.5]_{\text{stars}} < 0$, whereas contaminants have colors with $[3.6] - [4.5]_{\text{dust}} > 0$. In this chapter, we discuss trends in the stellar and non-stellar images of our sample LSB galaxies, propose improvements to our methods, and consider future work to be done on this project.

5.1 Dust Emission Content

The non-stellar images for all 10 galaxies in our sample revealed that there was always at least some dust emission present. Warm dust emission only shows in the non-stellar image if

there are young stars to heat it up. Because the non-stellar images indicate that there is dust emission, correspondingly, there must also be young stars forming.

In the analysis of high surface brightness (HSB) galaxies in the S⁴G conducted by Querejeta et al. (2015), the main component in the non-stellar images was “diffuse dust.” This type of dust is spread evenly throughout the galaxy and is a mixture of PAH and the dust continuum. Based on visual inspection of our non-stellar images, it appears that diffuse dust is not seen in our sample; all the dust in our sample is associated with large star-forming HII regions. Because visual inspection is not sufficient, we hope to measure the content of diffuse dust in LSB galaxies in the future. This can be done by subtracting total dust emission from the entire galaxy to the sum of the dust emission from the HII regions. We hope to use our results to compare diffuse dust in LSB galaxies with HSB galaxies.

5.2 Location of Old Stellar Population

High surface brightness (HSB) galaxies follow the “inside-out” theory of galaxy evolution, forming stars in the inside regions first and then spreading outward to the outer regions. This is because with the much more rapid speed of matter near the center and a shorter dynamical time, it is easier to start the formation of a galaxy in the core. In our sample, like their HSB counterparts, all stellar images indicate that old stellar populations in LSB galaxies are in the center.

5.3 Location of Star Formation

Because star formation starts in the center for high surface brightness (HSB) galaxies (and also lasts the longest there), the center should contain higher concentrations of heavier elements. Therefore, HII regions are likely to be found in the center. This same pattern is not seen in our data. In our ten galaxies, there are a small number of HII regions with no preference for the centers of the galaxies, which is quite noticeable in UGC 5709 and F584-2. A possible explanation for this result is that LSB galaxies have a chemical composition that is the same everywhere. Because of this, the enrichment can happen in any direction, resulting in HII regions that are formed in random locations. It is unclear why this trend occurs in LSB galaxies.

5.4 Improvements

Several steps should be taken in order to refine our method. In this section, we suggest three of these improvements.

5.4.1 Signal-to-Noise Threshold

Instead of setting the signal-to-noise (S/N) ratio threshold by eye (step 5 in the procedure), it would have been better to determine this threshold value by calculating the signal-to-noise in each image. The signal is the number of photon counts from the galaxy that falls within the aperture. There are four main sources of noise: read noise, dark current noise, shot noise in source, shot noise in sky. Once we have these values, we can determine if the pixel has a $S/N > 10$, which Meidt et al. (2012) and Querejeta et al. (2015) calculated to be the cutoff.

5.4.2 Masking Foreground Stars

Another possible improvement to the method is to find a suitable way to determine which stars are part of a galaxy and which are not. This can be hard to decide if there are many stars in the field of view. In step 6 of the procedure, we distinguished between field stars and background galaxies by visually comparing the available color images in the SIMBAD and SDSS astronomical databases. Masking any objects that are not part of the galaxy is crucial because ICA is sensitive to outliers. A better solution would have been to use SExtractor, a software package for detecting astronomical sources. Although this route is effective, there is always the potential that the software will pick up stars that are not part of the galaxy. We could then put constraints on which stars will be picked up by using ultra-violet and VIRUS-P data or by modifying the resulting image by eye.

5.4.3 Applying a Second Iteration of ICA

After the images have gone through the first iteration of Independent Component Analysis (ICA), Querejeta et al. (2015) examined the colors of the resulting non-stellar images, stating that the ICA favors hot dust which can lead to overestimation. If the pixels did not fall within the expected ranges of dust, these same pixels in the input images were masked. A second iteration was then performed on the updated masked images. Masking extreme colors and flux outliers can reveal different components of the galaxy. In the future, we would like to implement this second iteration because this project used only one.

5.5 Future Work

This thesis establishes a foundation for applying the ICA technique to the study of other LSB galaxies. There are many future paths for this project as described below.

5.5.1 Dust Content Maps

To determine if LSB galaxies are truly overfed and to understand the effects of high velocity clouds, we could use the non-stellar images to determine the dust content in a galaxy. A non-stellar image does not account for all dust present in a galaxy; it only measures the content of warm dust, which is heated by young stars. To correct for this, we can divide each non-stellar image by the star formation rate (SFR) maps of the appropriate galaxy to account for cold dust. If we compare dust content with metallicity, we can then determine if LSB galaxies are overfed. LSB galaxies that have high dust content and a low metallicity are overfed, while LSB galaxies that have a high dust content and a high metallicity are not.

5.5.2 Mass Maps

Unbiased stellar images, free of contaminants can be converted into mass maps to show the distribution of mass within the galaxy. Mass maps are critical in understanding the distribution of baryons and the underlying physics that have shaped the galaxy. They would allow us to compare the observed rotation curves to estimate the distribution of dark matter in LSB galaxies and gain a better understanding of the interaction of dark matter. In addition, because LSB galaxies account for a large fraction of the galaxies in the universe (10-50%), constraining their mass could help to solve the missing mass problem (see Chapter 2). The technique for converting our stellar images to a mass map has already been laid out by Meidt et al. (2011)

5.5.3 Mass-to-Light Ratio

Our images will make it possible to calibrate a relationship between mass-to-light ratio (M/L) as a function of observed [3.6]-[4.5] color. To get this equation, we will create a graph of $\log(\text{mass}/L_{3.6})$ against the [3.6]-[4.5] color. The mass can be found using the stellar images. The $L_{3.6}$ and the [3.6]-[4.5] value can be found using the raw PBCD data that have been background-subtracted. The best fit line in the plot will be the $\log(M/L)$. This equation helps to determine the presence of dark matter because the mass that is accounted for is only the visible stellar population. We can compare our results with the mass-to-light ratio for for S⁴G, $\log(M/L) = -0.339(\pm 0.057) \times ([3.6]-[4.5]) - 0.336(\pm 0.002)$ (Querejeta et al. 2015).

5.6 Summary

Low surface brightness (LSB) galaxies have paradoxical properties, with blue colors but faint stellar populations and gas rich-disks with low star formation. These galaxies are laboratories into understanding quiescent evolution, dark matter, solving the missing mass problem, and understanding star formation in low metallicity environments. Their evolutionary path is not well-understood. They are believed to be the result of isolation, affected by dark matter or the outcome of galactic overfeeding. To test the latter, we created warm dust maps by decomposing the Spitzer IRAC 3.6 and 4.5 μm images using Independent Component Analysis in 10 LSB galaxies. Our results tell us that in these type of galaxies, warm dust is present, old stellar populations reside in the centers, and there are a small number of larger HII regions that do not show preference to the center, unlike their high surface brightness (HSB) galaxy counterparts. In the future, we hope to increase our sample size and refine our methods. There is

still a lot of work to be done towards understanding the full picture of the evolutionary path of low surface brightness (LSB) galaxies, but through this thesis, we have contributed a missing piece to the puzzle.

Bibliography

- Adami, C., Scheidegger, R., Ulmer, M., Durret, F., Mazure, A., West, M. J., ... & Picat, J. P. (2006). A deep wide survey of faint low surface brightness galaxies in the direction of the Coma cluster of galaxies. *Astronomy & Astrophysics*, 459(3), 679-692.
- Aniano, G., Draine, B. T., Gordon, K. D., & Sandstrom, K. (2011). Common-resolution convolution kernels for space-and ground-based telescopes. *Publications of the Astronomical Society of the Pacific*, 123(908), 1218.
- Australia Telescope National Facility. (n.d.). *Evolutionary Tracks Off the Main Sequence* [Artwork]. Retrieved from https://www.atnf.csiro.au/outreach/education/senior/astrophysics/stellarevolution_postmain.html
- Blain, A. W., Barnard, V. E., & Chapman, S. C. (2003). Submillimetre and far-infrared spectral energy distributions of galaxies: the luminosity—temperature relation and consequences for photometric redshifts. *Monthly Notices of the Royal Astronomical Society*, 338(3), 733-744.
- Bolatto, A. D., Simon, J. D., Stanimirović, S., Van Loon, J. T., Shah, R. Y., Venn, K., ... & Li, A. (2007). The Spitzer Survey of the Small Magellanic Cloud: S3MC Imaging and Photometry in the Mid-and Far-Infrared Wave Bands. *The Astrophysical Journal*, 655(1), 212.
- Bothun, G.D., Impey, C., & McGaugh, S. (1997). Low-surface-brightness galaxies: hidden galaxies revealed. *Publications of the Astronomical Society of the Pacific*, 109(737), 745.
- Bothun, G. D., Schombert, J. M., Impey, C. D., Sprayberry, D., & McGaugh, S. S. (1993). The small scale environment of low surface brightness disk galaxies. *The Astronomical*

- Journal*, 106, 530-547.
- Chung, A., Van Gorkom, J. H., O'Neil, K., & Bothun, G. D. (2002). Low Surface Brightness Galaxies and the Tully-Fisher Relation. *The Astronomical Journal*, 123(5), 2387.
- Comon, P. (1994). Independent component analysis, a new concept?. *Signal processing*, 36(3), 287-314.
- Das, M. (2013). Giant Low Surface Brightness Galaxies: Evolution in Isolation. *Journal of Astrophysics and Astronomy*, 34(1), 19-31.
- de Blok, W. J. G., & McGaugh, S. S. (1996). Does low surface brightness mean low density?. *The Astrophysical Journal Letters*, 469(2), L89.
- de Blok, W. J. G., McGaugh, S. S., & Van Der Hulst, J. M. (1996). H I observations of low surface brightness galaxies: probing low-density galaxies. *Monthly Notices of the Royal Astronomical Society*, 283(1), 18-54.
- de Blok, W. J. G., Walter, F., Brinks, E., Trachternach, C., Oh, S. H., & Kennicutt Jr, R. C. (2008). High-resolution rotation curves and galaxy mass models from THINGS. *The Astronomical Journal*, 136(6), 2648.
- de Vaucouleurs G., de Vaucouleurs A., Corwin H.G., et al., 1991, Third Reference Catalogue of Bright Galaxies. Springer, New York (RC3).
- Disney, M. J. (1976). Visibility of galaxies. *Nature*, 263(5578), 573-575.
- Ellis, G. L., Grayson, E. T., & Bond, H. E. (1984). A Search For Faint Planetary Nebulae on Palomar Sky Survey Prints. *Publications of the Astronomical Society of the Pacific*, 96(578), 283.
- Elmegreen, B. G., Seiden, P. E., & Elmegreen, D. M. (1989). Spiral arm amplitude variations

- and pattern speeds in the grand design galaxies M51, M81, and M100. *The Astrophysical Journal*, 343, 602-607.
- Elmegreen, D. M., & Elmegreen, B. G. (1984). Blue and near-infrared surface photometry of spiral structure in 34 non-barred grand design and flocculent galaxies. *The Astrophysical Journal Supplement Series*, 54, 127-149.
- Elmegreen, D. M., Elmegreen, B. G., & Bellin, A. D. (1990). Statistical evidence that galaxy companions trigger bars and change the spiral Hubble type. *The Astrophysical Journal*, 364, 415-419.
- Flagey, N., Boulanger, F., Verstraete, L., Deschênes, M. M., Crespo, A. N., & Reach, W. T. (2006). Spitzer/IRAC and ISOCAM/CVF insights on the origin of the near to mid-IR Galactic diffuse emission. *Astronomy & Astrophysics*, 453(3), 969-978.
- Foyle, K., Rix, H. W., Walter, F., & Leroy, A. K. (2010). Arm and interarm star formation in spiral galaxies. *The Astrophysical Journal*, 725(1), 534.
- Galaz, G., Herrera-Camus, R., Garcia-Lambas, D., & Padilla, N. (2011). Low Surface Brightness Galaxies in the SDSS: The Link Between Environment, Star-forming Properties, and Active Galactic Nuclei. *The Astrophysical Journal*, 728(2), 74.
- Galaz, G., Milovic, C., Suc, V., Busta, L., Lizana, G., Infante, L., & Royo, S. (2015). Deep Optical Images of Malin 1 Reveal New Features. *The Astrophysical Journal Letters*, 815(2), L29.
- Garn, T., & Best, P. N. (2010). Predicting dust extinction from the stellar mass of a galaxy. *Monthly Notices of the Royal Astronomical Society*, 409(1), 421-432.
- Hayward, C. C., Irwin, J. A., & Bregman, J. N. (2005). The cosmological unimportance of low

- surface brightness galaxies. *The Astrophysical Journal*, 635(2), 827.
- Hunter, D. A., Elmegreen, B. G., & Martin, E. (2006). Mid-Infrared Images of Stars and Dust in Irregular Galaxies. *The Astronomical Journal*, 132(2), 801.
- Hurt, R. (2005). *Polycyclic Aromatic Hydrocarbons* [Artwork]. Retrieved from <https://legacy.spitzer.caltech.edu/features/articles/20050627.shtml>.
- Hyvarinen, A. (1999). Fast and robust fixed-point algorithms for independent component analysis. *IEEE transactions on Neural Networks*, 10(3), 626-634.
- Hyvärinen, A., & Oja, E. (2000). Independent component analysis: algorithms and applications. *Neural networks*, 13(4), 411-430.
- Impey, C., & Bothun, G. (1997). Low surface brightness galaxies. *Annual Review of Astronomy and Astrophysics*, 35(1), 267-307.
- Kendall, S., Kennicutt, R. C., Clarke, C., & Thornley, M. D. (2008). Tracing spiral density waves in M81. *Monthly Notices of the Royal Astronomical Society*, 387(3), 1007-1020.
- Kennicutt Jr, R. C. (1983). The rate of star formation in normal disk galaxies. *The Astrophysical Journal*, 272, 54-67.
- Kim, J.H (2007). The Star Formation History of Low Surface Brightness Galaxies. Ph.D. thesis, University of Maryland.
- Knapen, J. H., Beckman, J. E., Heller, C. H., Shlosman, I., & De Jong, R. S. (1995). The central region in M100: Observations and modeling. *arXiv preprint astro-ph/9506098*.
- McGaugh, S. S. research website. *Research*. Retrieved from <http://astroweb.case.edu/ssm/research.html>
- McGaugh, S. S. (1992). The Physical Properties of Low Surface Brightness Galaxies. Ph.D.

thesis, University of Michigan

McGaugh, S. (1993). Oxygen abundances in low surface brightness disk galaxies. *arXiv preprint astro-ph/9311064*.

McGaugh, S.S. & Bothun, G. (1994). Structural characteristics and stellar composition of low surface brightness disk galaxies. *arXiv preprint astro-ph/9311003*.

McGaugh, S. S., Bothun, G. D., & Schombert, J. M. (1995). Galaxy selection and the surface brightness distribution. *arXiv preprint astro-ph/9505062*.

Meidt, S. E., Schinnerer, E., Knapen, J. H., Bosma, A., Athanassoula, E., Sheth, K., ... & Elmegreen, B. G. (2011). Reconstructing the Stellar Mass Distributions of Galaxies Using S4G IRAC 3.6 and 4.5 μm Images. I. Correcting for Contamination by Polycyclic Aromatic Hydrocarbons, Hot Dust, and Intermediate-age Stars. *The Astrophysical Journal*, 744(1), 17.

Meidt, S. E., Schinnerer, E., Muñoz-Mateos, J. C., Holwerda, B., Ho, L. C., Madore, B. F., ... & Sheth, K. (2012). The S4G Perspective on Circumstellar Dust Extinction of Asymptotic Giant Branch Stars in M100. *The Astrophysical Journal Letters*, 748(2), L30.

Meidt, S. E., Schinnerer, E., Van De Ven, G., Zaritsky, D., Peletier, R., Knapen, J. H., ... & Kim, T. (2014). Reconstructing the Stellar Mass Distributions of Galaxies Using S4G IRAC 3.6 and 4.5 μm Images: II. The Conversion From Light to Mass. *The Astrophysical Journal*, 788(2), 144.

Mihos, J. C., McGaugh, S. S., & De Blok, W. J. G. (1997). Dynamical Stability and Environmental Influences in Low Surface Brightness Disk Galaxies. *The Astrophysical Journal Letters*, 477(2), L79.

- Mo, H. J., McGaugh, S. S., & Bothun, G. D. (1994). Spatial distribution of low-surface-brightness galaxies. *Monthly Notices of the Royal Astronomical Society*, 267(1), 129-140.
- NASA/JPL-Caltech. (2016). *Anatomy of the Milky Way* [Artwork]. Retrieved from <http://sci.esa.int/gaia/58206-anatomy-of-the-milky-way/>
- NASA/JPL-Caltech/R. Hurt. (2003). *Spitzer Rendered Against an Infrared (100 Micron) Sky* [Artwork]. Retrieved from <http://www.spitzer.caltech.edu/images/3072-SIRTF-Spitzer-Rendered-against-an-Infrared-100-Micron-Sky>
- Nilson, P. (1973). Uppsala general catalogue of galaxies. *Uppsala Astron. Obs. Ann.*, 6.
- Norris, M. A., Meidt, S., Van de Ven, G., Schinnerer, E., Groves, B., & Querejeta, M. (2014). Being Wise I: Validating Stellar Population Models and M^*/L Ratios at 3.4 and 4.6 μ m. *The Astrophysical Journal*, 797(1), 55.
- O'Neil, K., Bothun, G. D., Schombert, J., Cornell, M. E., & Impey, C. D. (1997). A wide field ccd survey for low surface brightness galaxies. II. Color distributions, stellar populations, and missing baryons. *The Astronomical Journal*, 114, 2448.
- Pahre, M. A., Ashby, M. L. N., Fazio, G. G., & Willner, S. P. (2004). Mid-Infrared Galaxy Morphology Along the Hubble Sequence. *The Astrophysical Journal Supplement Series*, 154(1), 235.
- Peletier, R. F., Kutdemir, E., van der Wolk, G., Falc3n-Barroso, J., Bacon, R., Bureau, M., ... & Krajnovi3c, D. (2012). The SAURON project–XX. The Spitzer [3.6]–[4.5] colour in early-type galaxies: colours, colour gradients and inverted scaling relations. *Monthly Notices of the Royal Astronomical Society*, 419(3), 2031-2053.

- Pickering, T. E., Impey, C. D., Van Gorkom, J. H., & Bothun, G. D. (1997). Neutral Hydrogen Distributions and Kinematics of Giant Low Surface= 20 Brightness Disk Galaxies. *The Astronomical Journal*, 114, 1858.
- Querejeta, M., Meidt, S. E., Schinnerer, E., Cisternas, M., Muñoz-Mateos, J. C., Sheth, K., ... & Laurikainen, E. (2015). The Spitzer Survey of Stellar Structure in Galaxies (S4G): Precise Stellar Mass Distributions from Automated Dust Correction at 3.6 μm . *The Astrophysical Journal Supplement Series*, 219(1), 5.
- Regan, M. W., & Elmegreen, D. M. (1997). K-Band observations of barred spiral galaxies. *The Astronomical Journal*, 114, 965.
- Rosenbaum, S. D., & Bomans, D. J. (2004). The environment of low surface brightness galaxies. *Astronomy & Astrophysics*, 422(1), L5-L8.
- Salo, H., Laurikainen, E., Buta, R., & Knapen, J. H. (2010). Bars do drive spiral density waves. *The Astrophysical Journal Letters*, 715(1), L56.
- Schombert, J. M., Bothun, G. D., Schneider, S. E., & McGaugh, S. S. (1992). A catalog of low surface brightness galaxies-List II. *The Astronomical Journal*, 103, 1107-1133.
- Scoville, N. Z., Matthews, K., Carico, D. P., & Sanders, D. B. (1988). The stellar bar in NGC 1068. *The Astrophysical Journal*, 327, L61-L64.
- Sloan Digital Sky Survey. (n.d.). *Spiral Galaxies*. Retrieved from <http://cas.sdss.org/dr6/en/proj/basic/galaxies/spirals.asp>
- Van Der Hulst, J. M., Skillman, E. D., Smith, T. R., Bothun, G. D., McGaugh, S. S., & De Blok, W. J. G. (1993). Star formation thresholds in Low Surface Brightness galaxies. *The Astronomical Journal*, 106, 548-559.

- Wakker, B. (1999, December 14). *High Velocity Clouds and the Milky Way* [Image]. Retrieved from <http://apod.nasa.gov/apod/ap991214.html>.
- Willner, S. P., Ashby, M. L. N., Barmby, P., Fazio, G. G., Pahre, M., Smith, H. A., ... & Regan, M. W. (2004). Infrared Array Camera (IRAC) Observations of M81. *The Astrophysical Journal Supplement Series*, 154(1), 222.
- Young, J. E. (2017), The Star Formation History of a Low Surface Brightness Galaxy. *in preparation*.
- Young, J. E., Kuzio de Naray, R., & Wang, S. X. (2015). The distribution of star formation and metals in the low surface brightness galaxy UGC 628. *Monthly Notices of the Royal Astronomical Society*, 452(3), 2973-2983.
- Zaritsky, D., & Lo, K. Y. (1986). Evidence for nonaxisymmetric nuclear bulges in spiral galaxies. *The Astrophysical Journal*, 303, 66-75.

Appendix A

Python code to convolve images

```
import numpy as np
import glob
from astropy.io import fits
import time
import scipy
from astropy.convolution import Gaussian2DKernel, convolve
import time
import os

cropped_I1_img, hdr = fits.getdata("cropped_I1.fits", header = True)
cropped_I2_img, hdr = fits.getdata("cropped_I2_align.fits", header = True)

# to call the kernel images, needs to be an odd dimension
kernel_img_I1, chdr = fits.getdata("resampled-3.6_to_gaussian-2.5.fits", header = True)
numrows = len(kernel_img_I1)
numcols = len(kernel_img_I1[0])
print ("original length:", numrows, numcols)

if numrows % 2 != 0 and numcols % 2 != 0: # if the image is already an odd dimension
    kernel_img_I1 = kernel_img_I1[:, :] # use the full length of the image
else:
    if numrows % 2 == 0: # if numrows is an even number
        numrows = numrows - 1
        kernel_img_I1 = kernel_img_I1[1:, :]
    if numcols % 2 == 0: # if numcols is an even number
        numcols = numcols - 1
        kernel_img_I1 = kernel_img_I1[:, 1:]
    if numrows % 2 == 0 and numcols % 2 == 0: # if both are an even number
        kernel_img_I1 = kernel_img_I1[1:, 1:]
print (len(kernel_img_I1), len(kernel_img_I1[0]))

# to call the kernel images, needs to be an odd dimension
kernel_img_I2, chdr = fits.getdata("resampled-4.5_to_gaussian-2.5.fits", header = True)
numrows = len(kernel_img_I2)
numcols = len(kernel_img_I2[0])
print ("original length:", numrows, numcols)

if numrows % 2 != 0 and numcols % 2 != 0: # if the image is already an odd dimension
    kernel_img_I2 = kernel_img_I2[:, :] # use the full length of the image
else:
    if numrows % 2 == 0: # if numrows is an even number
        numrows = numrows - 1
        kernel_img_I2 = kernel_img_I2[1:, :]
    if numcols % 2 == 0: # if numcols is an even number
        numcols = numcols - 1
        kernel_img_I2 = kernel_img_I2[:, 1:]
    if numrows % 2 == 0 and numcols % 2 == 0: # if both are an even number
        kernel_img_I2 = kernel_img_I2[1:, 1:]

print (len(kernel_img_I2), len(kernel_img_I2[0]))

start = time.time()
convolved_I1_img = convolve(cropped_I1_img, kernel_img_I1, boundary = "extend",
normalize_kernel = False) # blurr the 3.6 image only
fits.writeto("gauss_I1.fits", convolved_I1_img, hdr, overwrite = True )
end = time.time()

print (((end-start)/60)/60, 'hours elapsed')
```

```
print("I1 image was successfully saved")
print ("")

start = time.time()
convolved_I2_img = convolve(cropped_I2_img, kernel_img_I2, boundary = "extend",
normalize_kernel = False) # blurr the 4.5 image only
fits.writeto("gauss_I2.fits", convolved_I2_img, hdr, overwrite = True )
end = time.time()

print (((end-start)/60)/60, 'hours elapsed')
print("I2 image was successfully saved")
print ("")
```

Appendix B

Python code to perform background subtraction

```
import numpy as np
import glob
from astropy.io import fits
import scipy
import scipy.signal
import os

'''The purpose of this code is to take an image and to background subtract it using 5
rectangular region files '''

def read_box_file (file):
    '''reads in the one rectangular region file and returns the x1, x2, y1, y2 for the
    image array size '''

    file = open(file) # reads in file

    region = file.readlines()[3] # only wants the 3rd line that states the box size info

    if region[:3] == "box":
        region = region[4:-4] # get only the 4 values that we need from the string
        region = region.replace(',', ' ') # replace commas with whitespace
        region = [float(x) for x in region.split()] # list comprehension: convert each
        value to a float :)
    else:
        print ("Region is not a box-size, please re-do region again")

    cen_x = region[0] # this is the center of the x-component
    cen_y = region[1] # this is the center of the y-component
    width = region[2] # width of the box
    height = region[3] # height of the box

    x1 = int(cen_x - (width/2))
    x2 = int(cen_x + (width/2))

    y1 = int(cen_y - (height/2))
    y2 = int(cen_y + (height/2))

    return x1, x2, y1, y2

print (glob.glob("*.fits"))

filename = input("what is the name of the file? ")
file, hdr = fits.getdata(filename, header = True)
os.system("ds9 " + filename + " -scale zscale &")
print ("Make at least 5 region files and save them")

region_files = glob.glob("*.reg") # this is a list of all the region files
print("There are", len(region_files), "region files found:", region_files) # prints out
the number of region files found
print ("")
bkg_ls = [] # this is a list of the median background values for each region file

for region in region_files:
    x1 = read_box_file(region)[0]
    x2 = read_box_file(region)[1]
    y1 = read_box_file(region)[2]
```

```

y2 = read_box_file(region)[3]

bkg_section = file[y1:y2, x1:x2] # only want to focus on this section of the image
median = np.median(bkg_section) # get the median value of this section
print(median)
bkg_ls.append(median) # append this value into the list

avg_bkg = np.mean(bkg_ls) # take the average background value
print("")
print("The average background level:", avg_bkg)

# save background subtracted the image
bkg_sub_img = file - avg_bkg
avg_bkg = np.round(avg_bkg,5) # round this value
fits.writeto( filename[:-5] + "_bkg_sub_" + str(avg_bkg) + ".fits", bkg_sub_img, hdr,
overwrite = True) # save the new file
print("The file was successfully saved")
os.system("ds9 " + filename[:-5] + "_bkg_sub_" + str(avg_bkg) + ".fits" + "&")

```


Appendix C

C++ code to perform ICA

```
// compile with:
// g++ ICA.cpp -o example -litpp -std=c++11 -lcfitsio obsidian.o umbra.o -lpng
region.o
// ./example <name of I1 image> <name of I2 image> <name of region of galaxy> <name of
region of masked stars>

#include <itpp/itbase.h>
#include <itpp/signal/fastica.h>
#include "umbra.hpp" // include the image library
#include "region.hpp" // include the region library

using namespace itpp;
using namespace umbra;
using namespace gneiss;
using namespace std;
using namespace reality;

int main(int nargs, char* args[])
{
    // variable declarations: this leaves space for these variables
    FlatImage<double> I1_img; // for the I1 image
    FlatImage<double> I2_img; // for the I2 image
    vector<double> I1_ls; // vector of doubles
    vector<double> I2_ls; // vector of doubles
    vector<int> x_ls; // the list of x values that are good
    vector<int> y_ls; // the list of y values that are good
    mat sources; // matrix of the sources in the image
    vector<Region*> region_list; // a region file of the galaxy
    vector<Region*> mask_list; // a region file of the foreground stars
    Region *region;
    mat mixing_coef; // in the text, it's A
    bool foundInMask; // this boolean determines if the pixel is found in mask regions

    //=====//

    // read in the images

    I1_img.fits_read(args[1]);
    I2_img.fits_read(args[2]);

    //=====//

    // Create areas that should/ should not be part of analysis:

    region_list = read_region_file(args[3]); // this is the region file of the galaxy
    region = region_list[0];

    mask_list = read_region_file(args[4]); // this is the region file of the background
stars that are TOO bright

    //=====//

    // modify the matrix so that is is HIGH S/N and does not include stars that are too
bright!

    for (int x=0; x < I1_img.width(); ++x) // loops through the x
```

```

for (int y=0; y < I1_img.height(); ++y) // loops through the y
  if (I1_img(x,y) > 0.0001 and I2_img(x,y) > 0.0001 and region -> within (x,y) and
      is_real(I1_img(x,y)) and is_real(I2_img(x,y)))
    // 0.0001 is the cut off as the low S/N, has to be within the galaxy and does not
    // include the bright stars

    {
      foundInMask = false; // initially set to false
      for (int m = 0; m < mask_list.size(); m++) // loop through the mask_list
        if (mask_list[m] -> within (x,y)) // if the x and y values are in the
            mask_list regions
          foundInMask = true; // set it that pixel to true

      if (foundInMask == false)
        {
          x_ls.push_back(x); // appending x & y index to list
          y_ls.push_back(y);
          I1_ls.push_back(I1_img (x,y)); // append the pixel at x & y -->
            a copy of the original data
          I2_ls.push_back(I2_img (x,y));
        }
    }

// create a matrix with 2 columns -- one for I1 and one for I2 & the same size as the
// images
sources.set_size(2, I1_ls.size(), false); // size = rows * columns , 2 images so 2
// columns

// loop over the whole image
for (int r = 0; r < I1_ls.size(); ++r)
{
  sources(0,r) = I1_ls[r]; // separates the I1, I2 --> sources
  sources(1,r) = I2_ls[r];
}

//=====//

double a1, b1, cstart, cstart2;
string to_string[5] = { "0", "1", "2", "3", "4"};
for(int q=0;q<3;q++){
  for(int p=0;p<4;p++){
    for(int pp=0;pp<4;pp++){

      // ITTP analog sources --> sources (deconvolved)
      Fast_ICA fastica(sources);
      fastica.set_nrof_independent_components(sources.rows());
      fastica.set_non_linearity(FICA_NONLIN_GAUSS);
      fastica.set_epsilon(.00001);
      fastica.set_mu(.001);
      fastica.set_max_num_iterations(10000);

      cstart=((.516+q*.0308)+.0154*(p+1)); //To provide the seed range stated in the
      paper (-0.2, 0) and (0, 1.5)
      cstart2=.64*(pp+1); //col1=-2.5*log(ZP/cstart),
      col2=-2.5*log(ZP/cstart2), where ZP=179.7/280.8
      b1=(.8-cstart)/(cstart2-cstart);
      a1=1-b1;

      //define start guess for mixing matrix
      mixing_coef.set_size(2,2, false);
      mixing_coef(0,0)=100*b1;
      mixing_coef(0,1)=100*a1;
      mixing_coef(1,0)=100*b1*cstart2;
      mixing_coef(1,1)=100*a1*cstart;

      fastica.set_init_guess(mixing_coef);

```

```

// Perform ICA
cout << " conversion = " << fastica.separate() << "\n";

mat ICs = fastica.get_independent_components();
mixing_coef = fastica.get_mixing_matrix();
cout<< "mixing coef:" << mixing_coef << "\n";

I1_img.assign(I1_img.size(), get_null<double>());
I2_img.assign(I2_img.size(), get_null<double>());

for (int r = 0; r < I1_ls.size(); ++r) // loop over the independent component
{
    // put the pixel back to where they came from (now that we are finish with
    decomposition)
    I1_img(x_ls[r], y_ls[r]) = ICs(0,r);
    I2_img(x_ls[r], y_ls[r]) = ICs(1,r);
}

I1_img.fits_write("deconvolved/I1_" + to_string[p]+ "_" + to_string[q] + "_" +
to_string[pp] + "_fits", OVERWRITE);
I2_img.fits_write("deconvolved/I2_" + to_string[p]+ "_" + to_string[q] + "_" +
to_string[pp] + "_fits", OVERWRITE);

}
}
}

return 0;
}

```